Abstract

Since the middle of the 80's, zirconia stabilized with yttrium oxide (Y-TZP) is used in order to produce femoral heads. This material shows a reinforcement mechanism by phase transformation that provides excellent mechanical properties. But, in humid atmosphere, a surface degradation exists, that damages the Y-TZP surface. This degradation corresponds to a phase transformation that increases the roughness and micro-cracking. This kind of phenomenon may engender the failure of femoral heads in vivo or its malfunction.

Moreover, as zirconia is subjected to friction, when used in biomedical applications as hip prosthesis, it is highly important to investigate the effect of aging sensitivity on wear behavior.

Nitridation presents an attractive procedure to protect zirconia against degradation because, when optimized, it can avoid the occurrence of this phenomenon and keep mechanical properties unchanged. The goal of the present work is to investigate the influence of nitridation of zirconia ceramics on their tribological behavior and its effect on the material. The study is based on the comparison of the behaviour between zirconia nitrided at 1400, 1500 and 1600°C. At 1600°C a harder t' phase layer with bigger grain size is formed, but very brittle and low fracture toughness. At 1400°C and 1500°C no change in morphology and mechanical properties were detected.

The present work shows the high resistance of nitrided zirconia against hydrothermal degradation, as nitridation temperature increases. This improved behavior of zirconia is the consequence of the increase of the amount of vacancies qt the surface, preventing reaction with water from environment. Concerning the wear behavior tests against 3Y-TZP elements, all nitrided samples showed coefficient of friction around 0,6; and their wear rates corresponded to mild wear regime. t-m transformation and plastic deformation were found to be the main wear mechanisms for nitridation at 1400 and 1500°C, whereas for 1600°C, when t' phase is formed, plastic deformation is dominant.

Summary

Preface

This Project takes place in the European curses of the EEIGM (European School of Materials Engineering). The objective is to make the students discover the research field and prepare them to work in this area. Laboratories belong to the material department of one of the four partner universities.

There are two main objectives into this project:

- Study the nitridation of 3Y-TZP and, more precisely, investigate the microstructure, the mechanical properties (Vickers hardness and fracture toughness), and its effect on resistance to hydrothermal degradation.

- Determine the wear behavior of surface nitrided zirconia against 3Y-TZP elements, in terms of wear mechanism, coefficient of friction and specific wear rate, according to different nitridation temperatures.

1. Introduction

1.1 Characteristics and properties of zirconia

1.1.1 Generalities

Zirconia is the common name of the zirconium oxide ZrO2, which has a white aspect. This material is a technical ceramic, used for engineering applications contrary to pottery which includes tableware, decorative art objects and sanitary ware; and it is well-known for having a wide range of interesting properties.

Concerning chemical properties, zirconia has a high biocompatiblity in-vitro as well as in-vivo and it is one of the reasons why zirconia is used in biomedical applications such as femoral heads and dental prosthesis. Furthermore, this ceramic presents a good stability in aggressive chemical environments and also a good ionic conductivity that makes it interesting for solid oxide fuel cells and gas sensors.

Zirconia is also used as a refractory thanks to its high melting point (around 2680°C), even if alumina and silica are better refractors than zirconia.

When the adequate microstructure is produced, the zirconium oxide (for two of its polymorphs: monoclinic and tetragonal) can achieve high strength (> 1 GPa) as well as a high fracture toughness (10 MPa.$m^{1/2}$) and a good wear resistance; this last is the second reason why zirconia is used in joint replacements. Those interesting faculties make zirconia a high-quality material in engineering applications.

The name of zirconia[1] comes from the Arabic zargon (“the color of gold”), which in its turn, comes from the Persian words zar (“gold”) and gun (“colour”). The zirconium oxide ZrO2 was discovered in 1789 by the German chemist Klaproth, who extracted it from zircon (ZrSiO4). Since then it has been used for a long period in mixtures with others rare earths.

This ceramic is extracted from two main natural minerals: baddeleyite, which always contains a small amount of HfO_2 (Hafnium oxide, a compound hard to eliminate), and $ZrSiO_4$ (Zircon). The latter represents the main source and can easily be found as sand in Australia and South Africa.

At ambient pressure, pure zirconia exhibits three polymorphs[2], each of them is stable at well defined and different range of temperatures: ZrO_2 has a cubic structure (fluorite, CaF_2) at high temperatures (over 2370°C), a tetragonal structure (t-ZrO_2) at intermediate temperatures (from 1200°C to 2370°C), and a monoclinic structure (m-ZrO_2) at low temperatures (lower than 950°C) [Fig. 1][3].

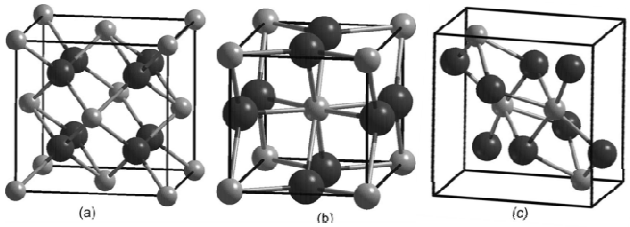

Figure 1: Conventional unit cells of the cubic (a), tetragonal (b), and monoclinic (c) ZrO_2 polymorphs; large dark spheres: O, small gray spheres: Zr.

1.1.2 Phase transformations

1.1.2.1 Tetragonal to monoclinic transformation

Tetragonal to monoclinic transformation belongs to the martensitic transformations, which occur in a number of metal alloys but also in minerals and ceramics like zirconia. This transformation happens, in pure zirconia, at 1000°C[4], it is associated with a large volume increase (around 4%) and shear strain and is favored when the material is exposed to humid environment.

It can be defined like the following way: ‘‘A martensitic transformation is a first order displacive structural transition exhibiting lattice invariant strain, which is essentially composed of a shear strain’’[5] .The first order displacive term means that the transformation

involves atomic displacements, that are small but finite (about a tenth of the atomic spacing), perfectly correlated and this for a large number of atoms.

During the transformation, no atomic diffusion is occurring, so that it may occur at any temperature, without changing either the atomic order or the chemical composition. The atomic shifts are such that they lead to a homogeneous strain of the crystal lattice, with a small volume change as compared to the shear components.

1.1.2.2 Transformation toughening

In general, transformation toughening is the increase in fracture toughness of a material that is the direct result of a phase transformation occurring at the tip of an advancing crack[6] [Fig. 2].

There are three essential requirements for successful transformation toughening. First, a metastable phase must be present in the material and the transformation of this phase to a more stable state must be capable of being stressed-induced in the crack-tip stress field. Secondly, the transformation must be instantaneous and do not require time-dependent processes such as long-range diffusion. Third, it must be associated with a change of shape and /or volume[6].

At the microstructural level, at the very crack tip, the toughening transformation may be schematically represented like on the figure 2.

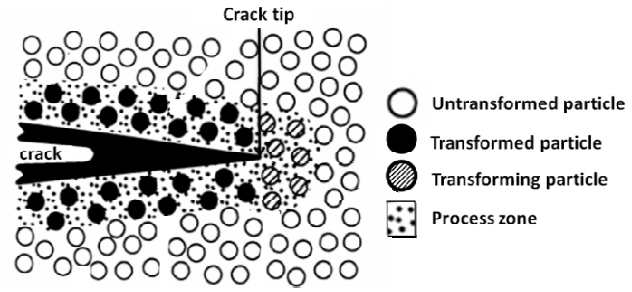

Figure 2: Transformation toughening

When a crack propagates through the material, the stress at the crack tip involves the tetragonal to monoclinic transformation, which implies a change of volume of 4% and also induces closing stresses to the crack. The propagation is then stopped and the fracture toughness is therefore increased.

This kind of transformation is observed in ceramics like zirconia, as well as in others materials such as shape memory alloys[7].

1.1.3 Stabilization

In order to retain zirconia in its metastable tetragonal structure at ambient temperature, it is possible to alloy it with various oxides[8] , like ceria (CeO_2), calcia (CaO), magnesia (MgO), rare earths and yttria (Y_2O_3). In the present work, zirconia was stabilized with the latter because of its mechanical properties, and its low price.

The reaction[8] occurring during the stabilization process with Y_2O_3 is the following.

$$Y_2O_3 + 2Zr_{Zr}^{x} + O_O^{x} \leftrightarrow 2Y_{Zr}^{'} + V_O^{\cdot\cdot} + 2ZrO_2 \qquad \text{(Eq.1)}$$

In this equation, Z_{Zr}^{x}, O_o^{x}, Y_{Zr}' and $V_o^{\cdot\cdot}$ denote zirconium cation on a regular zirconium site, oxygen anion on a regular oxygen site, yttrium cation replacing a zirconium cation and oxygen vacancy in the anionic sublattice, respectively.

The high temperature t-ZrO_2 phase is stabilized at room temperature by the presence of oxygen vacancies. The phase diagram of yttria-zirconia is shown on figure 3, which shows the two main families of zirconia stabilized with yttria, according to the microstructure. The comparison of the main properties of these two categories is presented in table 1.

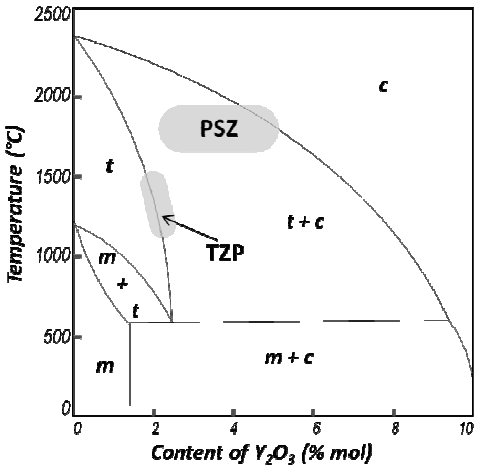

Figure 3: yttria-zirconia phase diagram

	Y-TZP	**Y-PSZ**
type of material	polycrystalline tetragonal zirconia	partially stabilized zirconia
content of stabilizer	2 – 3 mol% of Y_2O_3	6 – 10 mol% of Y_2O_3 [9]
grain size	0,2 - 0,5 µm [9]	~ 1 µm
hardness (Hv)	~ 12 GPa	~14 GPa
bending strength	> 950 MPa	> 500 MPa
fracture toughness	4-5 MPa. $m^{1/2}$	> 10 MPa. $m^{1/2}$ [9]

Table 1: properties of TZP and PSZ ceramics

The content of stabilizer in Y-TZP is 2 or 3 times smaller than the content of Y_2O_3 in Y-PSZ, which consists of a cubic ZrO_2 matrix with a dispersion of tetragonal precipitate. As Y-PSZ has a higher grain size and presents higher amount of cubic phase, it has a smaller strength than Y-TZP. The material used in this study belongs to the TZP (Tetragonal Zirconia Polycrystals) family, which presents good combination of properties: moderate fracture toughness and high strength [Tab. 1], and also low thermal conductivity, good ionic conductivity, and excellent wear behavior.

Equation 1 shows that one mole of yttria produces one mole of anion vacancies, and the total amount depends on the phases present. Table 2 shows that the concentration of vacancies is higher for cubic phase, followed by tetragonal, and for monoclinic phase is the minimum. The values shown are not strictly defined.

Phase	m	m + t	t	t + c	c
Amount of vacancies (%)	< 1,5	1,5 – 1,7	1,7 – 3,3	3,3 – 8	> 8

Table 2: vacancies amount in the different polymorphs of zirconia (m: monoclinic phase, t: tetragonal phase, and c: cubic phase)

The hydrothermal degradation, which zirconia suffers in with contact with water (see § 1.2), is known to be retarded with the amount of stabilizer[10] and becomes negligible when the molar percentage of yttria, in which the main phase is cubic, is higher than 6 mol %. In the present study, yttria is used at 3 mol % (5.2 wt %) [Fig. 3].

1.2 Hydrothermal degradation

1.2.1 Characteristics

Zirconia exhibits an unusual spontaneous transformation from tetragonal to monoclinic phases when it is exposed to humid environment. The consequence of this microstructural change is the production of microcraking, that is the cause of severe degradation of strength[11] and of dramatical loose in other mechanical properties. This modification at the surface of zirconia is called hydrothermal degradation or LTD (Low Thermal Degradation).

There are many conflicting and confusing mechanisms for modeling this particular ageing behavior of Y-TZP. Ageing observations have been explained using various mechanical and chemical degradation models but, in each case, the following features have been established:

(i) The tetragonal to monoclinic transformation starts from the surface and goes into the bulk[12,13].

(ii) Of all the major constituents that are in the air, only water vapor is responsible for the tetragonal to monoclinic transformation[11] **,** and the degradation is greatly accelerated by the presence of water[13].

(iii) The lower amount of dopant, the less the stability against the low thermal degradation[11].

(iv) The density has a significant effect on the degradation. If the density is greater than a critical value (Y_2O_3 dependent), then ageing will be drastically reduced[14].

(v) The degradation is time exposure and is favored at 200-300°C.

Hydrothermal degradation begins at the surface. The transformation[15] is an autocatalytic reaction: it leads to an increase in the volume, then, the transformed grain exerts strains on its neighbors, which induces microcracks. After that, water present in the

ambient environment is able to penetrate into the microcracks and reaches the material bulk. At the surface, gain pull-out can be observed when sliding is involved [Fig. 4]. Hydrothermal degradation can be described as a nucleation and growth reaction.

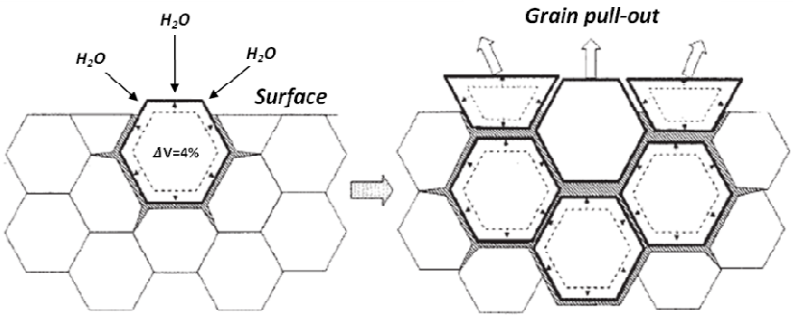

Figure 4: Aging process

At the atomic level, this transformation starts by the adsorption of H_2O at the ceramic surface [Fig. 4]. H_2O then reacts with O_2 from the surface in order to form OH^- ions. Those latter are then diffused towards the bulk. The vacancies, which are in zirconia thanks to stabilization, are annihilated, and the tetragonal to monoclinic transformation occurs.

1.2.2 Kinetics

Concerning the kinetics aspect of the low thermal degradation, numerous studies have been performed. Depending on the authors, the laws giving the monoclinic phase amount versus time can be either linear or sigmoidal (i.e. "S" shape). Many studies have been done about the latter[16,17], and they showed that this law is related to nucleation and growth kinetics (i.e. nucleation of the monoclinic phase first on isolated grains on the surface, then propagation to the neighboring grains as a result of stresses and microcracks accumulation). The kinetics of this sigmoidal law can be written using Mehl-Avrami-Johnson (MAJ)[18] expression, shown in equation 2.

$$f = 1 - e^{-(bt)^n} \quad \text{(Eq. 2)}$$

In this equation, *f* represents the monoclinic fraction, *t* is the aging duration and *b* corresponds to a parameter dependent on temperature. The exponent *n* of the equation 2 has been found to vary from 0,3 to almost 4 depending on the literature references. But Christian[18] tried to explain those different values by suggesting the existence of different mechanisms. In 2003, Gremillard and co-workers[18] have shown that this exponent *n* is not only characteristic of the aging mechanism (i.e. nucleation and growth), but also strongly dependent on the kinetic features (mainly nucleation speed and interface-or growth-speed).

1.2.3 Femoral heads

In 1985, Saint Gobain Desmarquest[4] first introduced 3Y-TZP in orthopedic field. This was to propose an alternative to alumina.

From 1985 to 2000, the French company sold more than 350,000 hip joint heads (under the name Prozyr®) worldwide. Within this period, only 28 brittle fractures were reported, representing a fracture rate of less than 0.01% (1 per 10,000 units). With the systematic use of proof tests on all implants in the middle of the 90's, the fracture rate even fell to 0.002% (1 per 50,000 units). Zirconia was therefore considered the second generation of ceramic hip joint heads, providing low wear rates and high safety.

In January 1998, to address the increasing commercial demand of zirconia hip joint heads, the company introduced a tunnel furnace instead of the usual batch furnace (kiln). A tunnel furnace provides a continuous sintering operation, leading to a reduction of processing time for larger series. The new hip joint heads were called TH-balls, whereas the previous were BH-balls.

By the end of 2000, two major orthopedic companies (Depuy France and Smith and Nephew) reported an unusual brittle fracture rate for zirconia TH-balls: 356 fractures were reported, corresponding to a mean failure ratio of 8% (up to 36% for batch TH-93038). This was a dramatic difference from the overall fracture rates reported in the prior 15 years. The French Medical Agency immediately suspended sales of the TH-balls. Given these concerns,

and because thousands of TH-balls had already been implanted in patients, the manufacturer, the major customers, and the French Medical Agency independently formed several groups of experts to answer the following questions:

(i) What was the cause (material, process, or design related) of the failures?

(ii) What difference between BH- and TH-balls led to a dramatic decrease in safety?

(iii) Why did the companies quality-control checks (density, grain size, mechanical strength testing, accelerated aging tests) not detect the vulnerability of TH-balls to delayed failure?

(iv) What was the risk of failure for patients with an implanted TH-ball?

Because the failures did not occur with BH-balls for identical designs, the problem was related to the process, more precisely to the change of the sintering furnace. The main differences lie in the sintering cycle and atmosphere, giving rise to a difference in microstructure. The thermal cycle applied on TH-balls likely leads to a lower intermediate density after sintering. More importantly, an uneven radial distribution of density may have occurred owing to the combination of cold isostatic pressing for the powder compaction and sintering in the tunnel furnace.

The critical events of 2001 may have been due to a combination of (i) the residual stresses and the presence of a lower density in the core region, where the taper is drilled, and (ii) an unexpected aging rate and the growth of aging-induced defects in a region in which tensile stresses are maximum. In other words, aging was proceeding very fast in a region in which no quality control was possible.

Owing to this critical event, a number of studies have now clearly assessed the role of density and residual stresses on aging. The example of the TH-balls shows that it is essential to continue experimental researches about zirconia used in biomedical applications.

1.2.4 How to avoid degradation

In order to avoid the low thermal degradation, Lawson[14] explains the different possibilities to prevent zirconia from ageing. Its review shows five ways to avoid hydrothermal degradation[14].

1.2.4.1 Chemical free energy increase

An increase in the chemical free energy can be achieved by increasing the yttria content. But unfortunately, this over-stabilization of the t-ZrO_2 phase (and probable c-ZrO_2 phase formation) leads to a reduction in the mechanical properties.

An alternative method of increasing the thermal stability of Y-TZP is to alloy with another stabilizing oxide. Sato and Shimada[19] examined the effects of different oxide additions. They observed that CeO_2 was an effective additive in order to eliminate degradation, without any reduction in mechanical properties and even an increase in the elastic modulus. TiO_2 did reduce the phase transformation but its addition increases grain size and reduces density, hardness and fracture toughness. The other oxides CaO and MgO did decrease the surface monoclinic content, but only because of increased cubic formation, which lowered the fracture toughness.

1.2.4.2 Strain free energy increase

Sato and co-workers[20] added from 5 to 10 wt% of Al_2O_3 to 3 mol% Y-TZP and found that the surface monoclinic content decreased with increasing concentration of dispersed Al_2O_3. They postulated that the Al_2O_3 grains play a major role in resisting the volume expansion of the zirconia grains accompanying the tetragonal to monoclinic phase transformation. Sato and Shimada[19] showed, in further investigations, that Al_2O_3 additions reduced the rate of transformation, and increased the elastic modulus. Schmauder and Schuberti however,

argue that additions of Al_2O_3 create stresses with the bulk ceramic which are detrimental to the ageing behavior of TZP. Masaki[21] supports this argument and includes TiO_2 and Fe_2O_3 into this category of stress raisers.

1.2.4.3 Surface free energy increase

The grain size of Y-TZP can be controlled by reducing the sintering temperature. However, unless the powders are ultra fine and highly reactive, the sintered density will not be very high. Hot-pressed or hot-isostatically pressed powders enable a small grain sized, fully dense Y-TZP to be manufactured.

A cheaper technique is the use of sintering additives to provide a small grain size through lowering the sintering temperature. The effect of additives on the anti-degradation behaviour of Y-TZP has been investigated by Kimura and co-workers[22] and Lawson and co-workers[23], transition metal oxide additives were used as sintering aids and resulted in densification occurring at about 1200°C. The doped 2,5 mol% Y-TZPs have a small grain size, were fully dense and were resistant to degradation in air and boiling water[22].

1.2.4.4 Coating

Iio and co-workers[24] coated Al_2O_3 onto the surface of Y-TZP. This sample was then aged in air at 300°C and they found that the tetragonal to monoclinic phase transformation had been restrained. Such coatings can be produced by CVD (Chemical Vapor Deposition) but processing is complicated and expensive. If the coating degrades or is fractured in any way, then the tetragonal grains will be open to water vapor attack.

1.2.4.5 Surface microstructural engineering

Whalen and co-workers used surface recrystallization in order to form a surface layer of very fine-grained tetragonal phase on Y-TZP[25]. This had the effect of resisting ageing at 200°C in air for 1000 h. Therefore large grain sized Y-TZP for maximum toughness can be protected from the tetragonal to monoclinic transformation by post-sintering treatments.

1.2.4.6 Choice of procedure to avoid degradation

In the present work, nitridation has been found to be the best way to avoid the hydrothermal degradation. In all the other methods described above, the addition of oxides would lead to a new material with different properties and would require other experimentations to determine them. Decreasing the grain size would engender a decrease in the fracture toughness. Concerning the coating method, attachment and incompatibility problems would eventually be to consider and avoid. Nitridation can be defined as a kind of surface microstructural engineering method: it results in the structural change at the surface of the material treated.

.

1.3 Nitridation

In recent times, it has been proposed that the low thermal degradation of yttria doped zirconia can be prevented by using a method, which is called nitridation. This process corresponds to the sintering or a heat treatment of ZrO_2 in presence of solid or gas source of nitrogen.

1.3.1 On pure zirconia

In pure ZrO_2, this process occurs at temperatures between 1400°C and 2200 °C in nitrogen atmosphere leading to the formation of zirconium oxynitrides[26,27] (nitrogen-containing zirconia). The nitridation is processed in nitrogen atmosphere, with the possibility of mixing with ZrN powder either the zirconia powder or coating sintered samples, Zirconium nitride (ZrN) is a greenish powder and its melting point is at 2980°C**.**

The nitridation process is more efficient when the material is compacted in ZrN powder than when there is only N_2 gas. However, there are two different contributions, one from the ZrN powder, and the other one from the nitrogen. The corresponding reactions occurring during the nitridation are the following[28]:

$$3O_O^x + 2N(ZrN) \rightarrow 2N_O^{'} + V_O^{\cdot\cdot} + 3O(ZrN) \qquad \text{(Eq. 3)}$$

$$3O_O^x + N_2(g) \rightarrow 2N_O^{'} + V_O^{\cdot\cdot} + \frac{3}{2}O_2(g) \qquad \text{(Eq. 4)}$$

In these equations, the following symbols are used: O_o^x is the oxygen contribution from zirconia, $V_o^{\cdot\cdot}$ represents the oxygen vacancies and N_o corresponds to a nitrogen anion replacing an oxygen anion.

The equation 3 describes the superficial solid-solid reaction, with the transport of nitrogen and oxygen atoms (or ions) between the ZrN powder and zirconia.

In equation 4, the reaction between solid and gas is described. This reaction involves complicated reactions steps: adsorption (desorption), dissociation (association), and charge transfer process. Therefore, the energy barrier for the nitridation process through the reaction 4 is higher than that of the reaction 3, which may explain the difference in nitridation kinetics.

The nitridation of pure ZrO_2 with ZrN and nitrogen gas produces three oxynitride phases in the zirconium oxynitride Zr-O-N system: γ phase is Zr_2ON_2, β phase is $Zr_7O_8N_4$ and β' is $Zr_7O_{11}N_2$[27].

The concentration of oxygen vacancies is, in the case of pure zirconia, smaller than for yttria doped-zirconia because it only takes into account the one produced by ZrN powder, whereas when zirconia is stabilized, this concentration is the addition of the oxygen vacancies from nitridation and the one formed by the presence of yttrium in the material[8].

Furthermore, the nitridation of pure zirconia leads to the formation of oxygen vacancies that are ordered, contrary to doped zirconia which oxygen vacancies are disordered. As the latter are not distributed randomly in the structure, in addition to γ, β and β', a new phase β'' is formed. This new structure is unknown but similar to β'[27].

1.3.2 On zirconia doped with yttria

1.3.2.1 In the bulk

Whether the nitridation process is described as in the equation 3 or as in the equation 4, the oxygen vacancies $V_o^{\cdot\cdot}$ generated by the incorporation of nitrogen into Y-TZP N_o' are known to stabilize the cubic phase. In commonly used partially stabilized ZrO_2, oxygen vacancies are formed to compensate the doped cations, in this case: Y_{Zr}'. The nitrogen incorporation and the consequent generation of oxygen vacancies involve the transformation of the TZP surface into the stable cubic phase.

The cubic phase formation at lower temperature in the case of nitridation is due to the convergence of the lattice parameters of ZrO_2 with the quantity of introduced nitrogen [Fig. 5]. The values of figure 5 correspond to the results of Cheng and co-workers[29] for nitriding 2 hours in nitrogen gas for a range of nitridation temperatures from 1500°C to 2000°C presented in table 3.

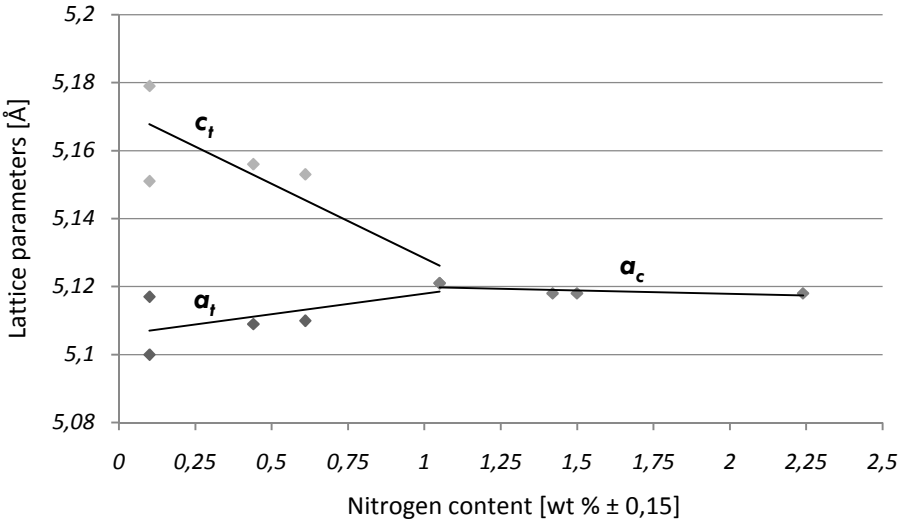

Figure 5: variation of the lattice parameters as a function of nitrogen concentration

Nitridation temperature is an essential parameter in this procedure. Table 3 shows the results of Cheng and co-workers[29], who studied the effect of nitridation temperature on the phases and the lattice parameters, for the same time of nitridation (2 hours) with nitrogen gas. For temperature lower than 1650°C, tetragonal and monoclinic are the two phases present in the bulk of the material. a_t and c_t converge and the tetragonality varies from 1,0149 for the raw material to 1,0084 for 3Y-TZP heat treated at 1650°C. Above 1700°C, the main phase found in the samples is the cubic phase and for a nitridation temperature of 2000°C, ZrN is present in the material.

Sintering conditions	*Phases**	a_t (Å)	c_t (Å)	a_c (Å)	c_t / a_t	*N (wt % ± 0,15)*
Raw material	*t*(vs), *m*(w)	5,102	5,178		1,0149	
1300°C/2h, N_2	*t*(s), *m*(mw)	5,105	5,179		1,0145	
1400°C/2h, N_2	t_1(s)	5,101	5,178		1,0151	
	t_2(w)	5,122	5,144		1,0043	
	m(mw)					
1500°C/2h, N_2	t_1(ms)	5,100	5,179		1,0155	0,10
	t_2(ms)	5,117	5,151		1,0066	
	m(mw)					
1600°C/2h, N_2	*t*(vs), *m*(vw)	5,109	5,156		1,0092	0,44
1650°C/2h, N_2	*t*(vs)	5,110	5,153		1,0084	0,61
1700°C/2h, N_2	*c*(vs), *t*(mw)			5,121		1,05
1750°C/2h, N_2	*c*(vs), *t*(vw)			5,118		1,42
1800°C/2h, N_2	*c*(vs)			5,118		1,50
2000°C/2h, N_2	*c*(vs),			5,118		2,24
	ZrN(mw)			4,576		

Table 3: Dependence of the temperature nitridation on the phases, the lattice parameters, and nitrogen content (*where *c* is cubic, *m* is monoclinic, *t* is tetragonal, *vs* is very strong, *s* is strong, *ms* is moderately strong, *mw* is moderately weak, *w* is weak and *vw* is very weak)

Sintered Y_2O_3 stabilized ZrO_2 usually consists of separate cubic and tetragonal grains, when the Y_2O_3 content exceeds the solubility limit[30,31].

During the sintering of 3Y-TZP in a nitrogen atmosphere, polymorphic phases of ZrO_2 also appeared as separate grains, although the main phase was progressively changed from the tetragonal phase to, first, the t' phase and, then, to the cubic phase [Tab. 3].

1.3.2.2 At the surface

1.3.2.2.1 Phase changes

Chung and co-workers[32] studied the microstructure of yttria doped-tetragonal zirconia after heat treatment in a nitrogen atmosphere. They observed the formation of a surface layer with grains that were much larger in size than those of the interior [Fig. 6]. Using X-rays diffraction, they showed that the larger grain size in the surface layer was caused by a higher grain-growth rate of the cubic phase that was stabilized by nitrogen. Because this stabilization started at the surface and progressed into the interior, the surface layer had a gradient of grain size. When the cation stabilizer was introduced to the green bodies by an

embedding powder, the resulting stabilized surface layer contained a certain amount of pores, because of rapid grain growth of the stabilized phase. As explain in the previous paragraph, the nitridation temperature provides different microstructures to the material treated. This difference is shown on figure 6[28] where the grain size and depth increase from 1400°C to 1600°C for the same experimental conditions.

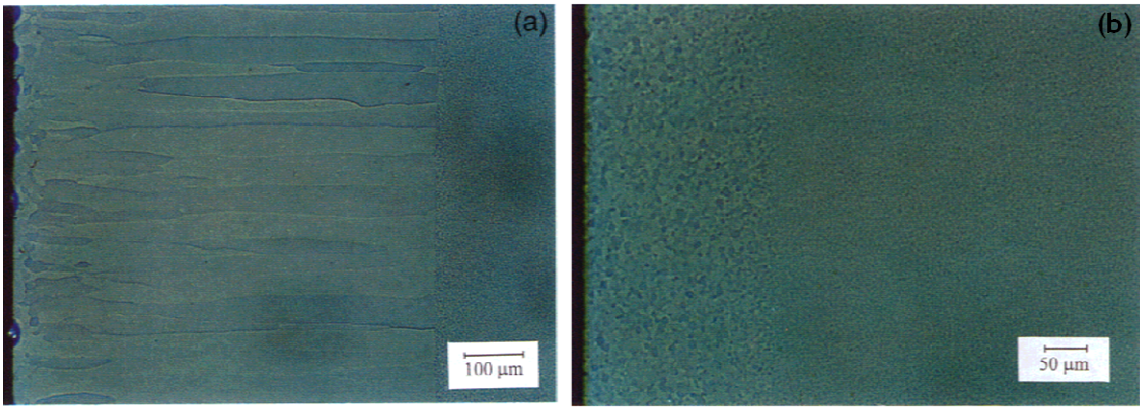

Figure 6: Micrographs showing the surface region of 2Y-TZP specimen after heat treatment with ZrN powder for 2 hours at (a) 1600°C, and (b) 1400°C

The nitrided 3Y specimens[32] do not show any phase transformation for the low-temperature annealing at 200°C for up to 400 h. The result indicates that the phases of the surface layer (cubic and non-transformable tetragonal t') are inert to the phase transformation, regardless of their stabilization mechanism.

1.3.2.2.2 Mechanical properties

Since nitrided zirconia exhibits improvements in its mechanical properties, some researches have been performed to explain and analyze those changes in more precise ways.

It has been shown[33] that the Vickers microhardness shows higher values in nitrided zirconia (~14 GPa) than in less- or non-nitrided material (~12 GPa): nitridation is time-dependant. The increase in hardness at the surface layers with time could be associated with

(i) a larger nitrogen content present in such regions, (ii) a larger grain size, and (iii) the presence of t' phase. Furthermore, the values of H_v decrease with the depth, as shown by Feder and coworkers[33] [Fig. 7], but it also depends on the nitrided time: above a certain exposure-time, which is related to the experimental conditions, H_v, at the very superficial layer, decreases and becomes smaller than in the inner layers. This change in the H_v values has been explained by the formation of a cubic layer in the outer nitrided layer. As the cubic grains are larger than the tetragonal grains, there is a loss of hardness in this part of the material.

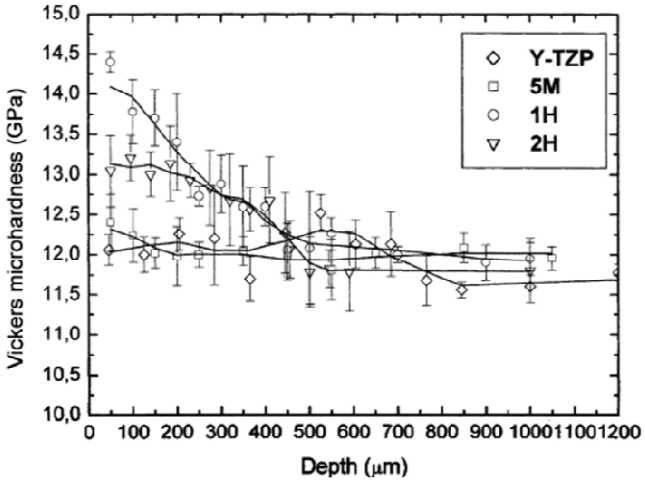

Figure 7: Vickers microhardness profiles of surface nitrided 2,5 Y-TZP as a function of depth for as-sintered zirconia, 5M (5 minutes), 1H (1 hour) and 2H (2 hours) at 1650°C

The yttria content can also have an influence on the hardness of the nitrided material. Chung and co-workers[32] showed that the hardness of the nitrided surface layer of the 3Y specimens heat-treated at 1600°C for 2 hours (13,8 ±0,2 GPa) was higher than either the as-sintered 3Y at 1600°C for 3 hours (13,3 ±0,2 GPa) and 8Y at 1600°C for 2 hours (12,7 ±0,1 GPa) specimens, which could be attributed to the increase of the oxygen vacancies due to the nitrogen dissolution.

Concerning the fracture toughness K_{IC}, Fischer and co-workers observed an increase in the bulk [Tab. 4] and this difference of values is, as for the hardness, explained by the different grain sizes.

Nitriding time	K_{IC} *(MPa.m$^{1/2}$)*
5 minutes	4,8
1 hour	5,5
2 hours	5,8

Table 4: dependence of nitriding time on the fracture toughness measured in the bulk (on 2,5Y-TZP specimen at 1650°C)

This increase in fracture toughness results from the decrease in the activation energy from tetragonal to monoclinic phase transformation under applied stresses (i.e. increase of the tetragonal grain size), contrary to the mechanism at the surface, where the fracture toughness decreases because of the presence of cubic phase.

Chung and co-workers[32] studied the fracture toughness of 3Y-TZP samples, heat-treated at 1600°C for 2 h in nitrogen atmosphere. They observed that the fracture toughness increases with the depth of the specimen: in the interior of the material, the fracture toughness was 5,0 ±0,3 MPa.m$^{1/2}$ whereas the value at the surface was 2,4 ± 0,2 MPa.m$^{1/2}$. This result is also explained by the difference of cubic phase at the surface layer.

1.3.2.2.3 Resistance to degradation

The resistance against hydrothermal induced phase transformation of nitrided specimens[33] has been studied by A. Feder and co-workers and compared to the results obtained for Y-TZP under similar conditions. In their investigations, they found out that nitrided samples degraded in boiling water (100°C) did not show any appearance of monoclinic phase after 900 hours of treatment. This finding indicates the non-transformable character of the microstructure at Y-TZP nitrided surfaces.

1.4 Tribological behavior of zirconia

1.4.1 Generalities

In order to improve properties of materials used in tribology, it has been shown that the only issue is to replace metallic materials by ceramics, because of their high hardness and excellent corrosion resistance. That is why, in recent years, structural ceramic materials have seen major growth in tribological applications[34].

1.4.1.1 Wear modes

Wear mechanism can be from different natures. For this reason and in order to understand it, it is essential to distinguish its fundamental features: (i) its morphological characteristics of the worn surfaces (appearance shifts), (ii) the conditions under which the prosthesis was functioning when the wear occurred.

It is possible to classify wear into two different categories according to the number of phases involved: single-phase and multiphase wear. In the first type of wear, a solid, a liquid or a gas moving relatively to a sliding surface has for effect to remove material from the wearing surface. Concerning the multiphase wear, it occurs as for the single-phase wear, but, in addition, a second phase is produced, such as particles or asperities[35].

There is no exact description of material wear behavior, but nevertheless it is possible to classify it into some broad types: abrasive, adhesive, fatigue, fretting, corrosive and erosive wears[36,37].

Abrasive wear results from the presence of hard particles or protuberances that are obliged to move against and along the solid surface. This kind of wear generally involves progressive loss of material, which is due to relative motion between the surface and a contacting material.

Adhesive wear is generated by the sliding of a solid surface along another one. This type of wear occurs when the asperities on mutually opposing surfaces become fused together and are then subsequently ruptured because of their relative motion.

Fatigue wear can be in macroscopic or microscopic form. The first one can occur in non-conforming machine elements in the form of pitting or rolling contact fatigue. Fatigue wear on a microscopic scale is associated with individual asperity contacts rather than with the single large region. Both types are so severe that they lead to failure.

Fretting wear results from the small amplitude oscillation that may occur between two surfaces in contact. This oscillation is generated by an external vibration, and, in general, it is caused by the cyclic stress to which one of the contact members is subjected causing another and usually more damaging aspect of fretting.

Corrosive wear is the result of a chemical reaction (usually oxidation) on a wearing surface. Corrosion products (usually oxides) have shear strengths different from those of the metal wearing surfaces from which they derived. The oxides tend to flake away, resulting in the pitting of working surfaces.

Erosive wear is caused by particles that impinge on a component surface (or edge), and, due to momentum effects, remove material from that surface. This kind of wear is particularly noticed in components with high velocity flows. Particles repeatedly striking the surface may also cause denting and eventual fatigue of the surface.

Concerning ceramics, wear behavior may also be classified according to another criterion, which is the severity of wear. In this second categorization, the wear behavior of ceramics has been divided into two categories: (i) the “mild” wear, and (ii) the “severe” wear.

(i) According to H.R. Pasaribu and co-workers[38], the *mild wear* is defined when a relatively smooth wear track was formed with a specific wear rate less than 10^{-4} $mm^3.N^{-1}.m^{-1}$[34]. The specific wear rate represents the normalized (regarding the load, N,

applied during the test) removed volume (mm^3) for the total covered distance called the sliding distance (m).

(ii) The ***severe*** wear is defined when rough wear track was formed with a specific wear rate[34] larger than 10^{-4} $mm^3.N^{-1}.m^{-1}$.

To be useful as a commercial tribological material, ceramics, in their applications, are not allowed to achieve a certain specific wear rate (10^{-4} $mm^3.N^{-1}.m^{-1}$)[34], which corresponds to the limit between the mild wear and the severe wear. The transition from mild to severe wear of ceramics depends on the operating conditions such as normal load, velocity and temperature, and material properties like grain size, mechanical and thermal material properties[38].

1.4.1.2 Wear characterization

In order to describe properly the wear behavior of a material and to obtain a better understanding of the results, some wear characteristics have to be defined. The main feature when performing tribological tests is the specific wear rate (in $mm^3.N^{-1}.m^{-1}$). Another characteristic that describes the wear behavior of a given material is the coefficient of friction. This concept has been first introduced by Leonardo Da Vinci and it is defined as the ratio of the friction force to normal load[35].

As an example, Fischer and co-workers[39] studied the tribological behavior of 3Y-TZP in air at room temperature. For a speed of 0,001 m/s, and a load of 9,8 N, the value of the wear rate was 5.10^{-6} $mm^3.m^{-1}$ and the coefficient of friction was 0,35. According to these results and to the fact that they observed rolled wear debris on the sample, they proposed that a plastic deformation occurs, forming grooves.

1.4.2 Difference of behavior with the nature of acetabular cup and femoral ball head

Depending on the couplings material, the characteristics of wear behavior are changed as shown on the figure 8[40]. It compares the wear rate of four different couplings: CoCr-on-Polyethylene, Alumina-on-Polyethylene, Alumina-on-Alumina and Zirconia-on-Zirconia. It appears that the coupling Zirconia-on-Zirconia, among the four couplings tested, is the most wear resistant.

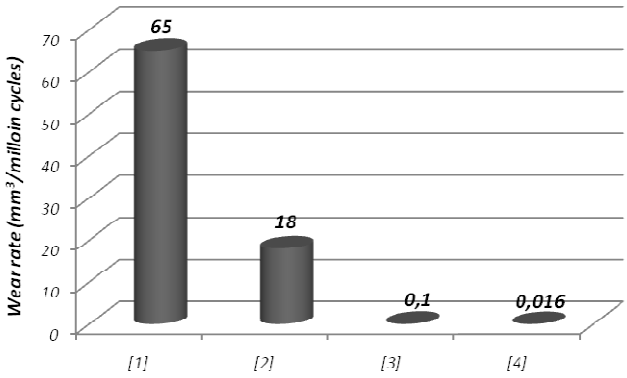

Figure 8: wear rate depending on the couplings, [1] CoCr-on-Polyethylene, [2] Alumina-on-Polyethylene, [3] Alumina-on-Alumina and [4] Zirconia-on-Zirconia

Concerning the experienced material in the present work, the wear behavior of zirconia has been observed by G. Willmann and co-workers[41]. Their study compares the following couplings: Y-TZP/Y-TZP and Y-TZP/Polyethylene (PE-UHMW). As shown on figure 9, the surface roughness profile of zirconia is much deeper when tribological tests are done between zirconia and itself, than between zirconia and polyethylene.

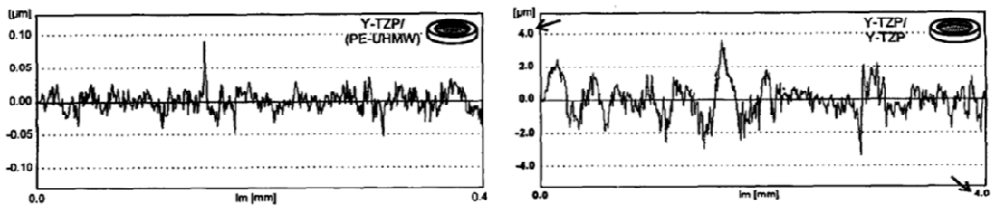

(a) Surface roughness profile of a zirconia ring (Y-TZP, running against PE-UHMW, $R_{y,max} = 0.140\,\mu m$, $R_a = 0.011\,\mu m$, $R_{pk} = 0.017\,\mu m$, $R_{vk} = 0.019\,\mu m$).

(b) Surface roughness profile of a zirconia ring (Y-TZP, $R_{y,max} = 6.210\,\mu m$, $R_a = 0.760\,\mu m$, $R_{pk} = 0.900\,\mu m$, $R_{vk} = 1.650\,\mu m$; for comparison to *Figures 1* and *2* note the different scale division.

Figure 9: difference of roughness between *(a)* Y-TZP/Y-TZP and *(b)* Y-TZP/Polyethylene

1.4.3 Difference of behavior between c- and t-phase

Travgott E. Fischer and co-workers[42] have performed tribological tests on ZrO_2-3 mol% Y_2O_3, ZrO_2-4 mol% Y_2O_3 and ZrO_2-6 mol% Y_2O_3. With these yttria contents, the material phases were fully tetragonal, mixed tetragonal and cubic, and fully cubic, respectively.

The results of their investigation are presented in the following table.

Yttrium content (mol%)	***Phase(s)***	***Fracture toughness ($MPa.m^{-1/2}$)***	***Specific wear rate (mm^3/Nm)***
3	*Fully tetragonal*	11,6	7.10^{-7}
4	*Tetragonal and cubic*	8,7	3.10^{-6}
6	*Fully cubic*	2,5	3.10^{-4}

Table 5: tribological characteristics of fully tetragonal, mixed tetragonal and cubic, and fully cubic zirconium oxides

Figure 10 shows that the fracture toughness has an extraordinarily large influence on its wear resistance, and more precisely, wear resistance of zirconia oxide increases with the fourth power of its fracture toughness.

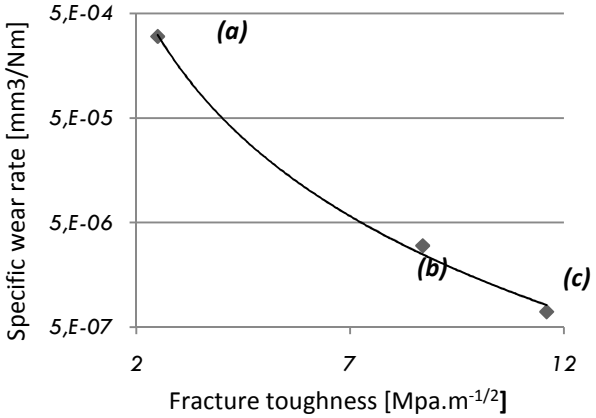

Figure 10: Variation of the specific wear rate on the fracture toughness of Y-TZP: (a) 6Y-TZP, (b) 4Y-TZP and (c) 3Y-TZP

2. Materials and experimental procedure

2.1 Samples preparation

2.1.1 Raw material

A commercial ZrO_2 powder containing 3 mol % Y_2O_3 (3Y-TZP) was used. This raw material has been imported from the Japanese firm TOSOH, and is commercialized in accordance with the standard ASTM-F1873, which refers to the morphological properties of zirconias used in biomedical field.

2.1.2 Compaction

The compaction of the powder has been performed by cold isostatic pressing (CIP). Polymeric mould containing 40 g of zirconia powder (white color) has been placed in ultrasonic for 10 minutes and then it has been cold isostatic pressed at 200 MPa for 3 to 5 minutes. Around 10 specimens were produced as described above to have enough samples to work. Cylinders of around 120 mm of length and 12 mm of diameter were obtained.

2.1.3 Sintering

The sintering has been processed with a tubular furnace Hobersal ST-18. During this step of material production, zirconia bars have been sintered following the procedure described on the figure 11. The first dwell at 600°C for 1 hour consists in eliminating the polymeric sintering additives from the powder. The second dwell is the sintering itself and was performed at 1450°C for 2 hours. For the all sintering procedure, the heating and the cooling rate were 3°C/min. At the end of the sintering step, bars of 80 mm of length and 8 mm of

diameter were obtained, and they have been cut into discs of 2 mm of thickness, using an automatic STRUERS Accutom-50.

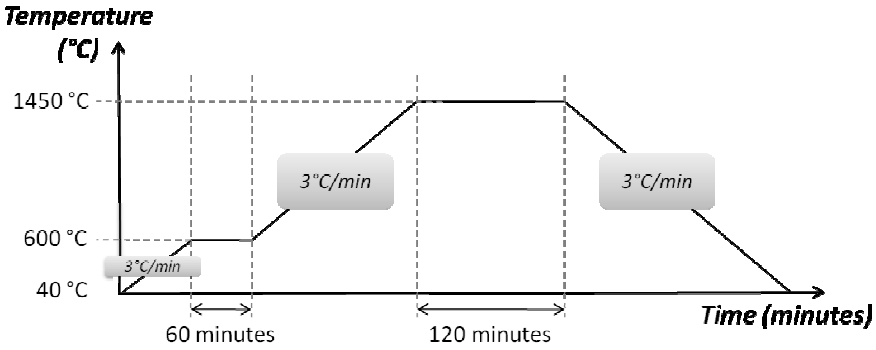

Figure 11: scheme of sintering process

2.1.4 Polishing

In order to properly polish zirconia samples, an automatic polishing machine Struers RotoPol-31 has been used. 7 discs are glued on bigger aluminum disc [Fig. 12] to make a faster polishing.

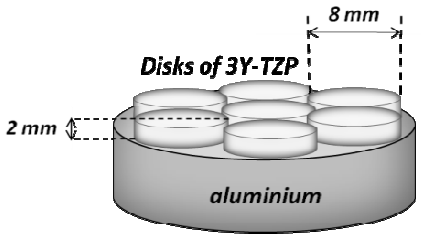

Figure 12: zirconia disks glued on aluminum plinth

Polishing has been processed in several steps as shown in the table 6.

	Glove	*Paste*	*Lubricant*	*Speed (rpm)*	*Duration (min)*	*Load (N)*
1	Petro disk 220-Sic (Struers)	-	H_2O	300	5 (to eliminate defects from the cutting step)	With hands
2	Struers MD Dac (white cloth)	Diamand 30 µm	Lubricant	300	30 (to obtain one plan on all the disks)	20
3	Struers MD Dac (blue cloth)	Diamand 30 µm	Lubricant	300	60 (to eliminate scratches of the previous step)	15
4	Struers MD Dac (blue cloth)	Diamand 6 µm	Lubricant	150	30 (scratches only observable on the microscope)	10
5	Struers MD Dac (blue cloth)	Diamand 3 µm	Lubricant	150	30	10
6	Struers MD Dac (pink cloth)	Colloidal silica solution	Lubricant	150	30	5
7	Struers MD Dac (pink cloth)	-	H_2O	150	5 (to clean the samples)	With hands

Table 6: Polishing steps

2.1.5 Density

According to ASTM F – 1873 standards, the discs are required to have a density higher than 6,00 $g.cm^{-3}$. Using a XS205 DualRange balance, Archimede method has been applied and the densities found are shown in the table 7.

Experimental value ($g.cm^{-3}$)	**Theoretical value ($g.cm^{-3}$)**	**Relative density (%)**
6,036 ± 0,019	6,100	98,940

Table 7: disks density

The density of zirconia samples is higher than 6,000 $g.cm^{-3}$, the material is therefore correct to use.

2.2 Nitridation

Before nitridation process itself, zirconia disks have to be prepared: (1) samples are carefully cleaned, (2) they are embedded in 0,7 g of ZrN powder all over the surface as shown on the figure 13 (a), and (3) they are carefully placed in the refractory container [Fig. 13 (b)].

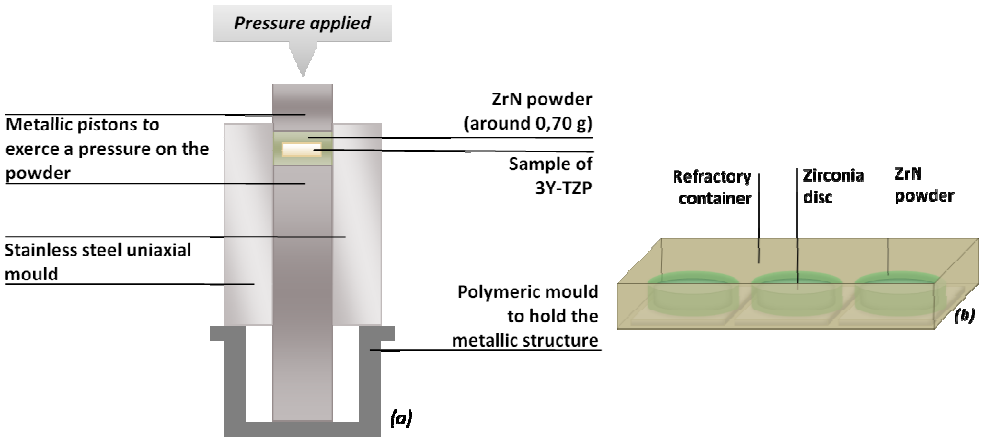

Figure 13: (a) compaction of zirconia disk into ZrN powder, (b) compacted zirconia/ZrN into a refractor container

Nitridation procedure has been performed with the same furnace as for the sintering, with a 100 % nitrogen atmosphere with a constant flux of 1 l/min. Zirconia samples have followed the nitridation process as shown on the figure 14. The doping has been performed for nitridation temperatures of: 1400°C, 1500°C and 1600°C. The heating and cooling rate used for this step of material production was 20°C/min.

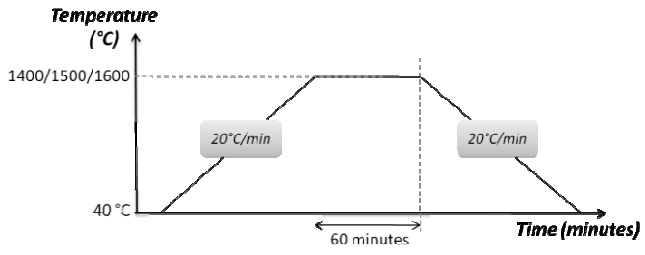

Figure 14: scheme of nitridation process

After nitridation procedure samples have been carefully removed from the furnace and they have been cleaned.

2.3 Degradation

Samples were placed in an autoclave P-Selecta in steam for 30 hours at 131°C and under 2 bar pressure, in order to artificially induce the phase transformation at the surface.

30 hours of such a treatment corresponds roughly to 90 year in vivo, according to S. Deville and co-workers who showed that 1 hour simulates about 3 year in vivo [43].

2.4 Tribology tests

Using a WAZAU TRM 1000 tribometer, ball-on-disk wear tests have been simulated [Fig. 15]. The parameters used for wear experiments are the following:

- Ball material : 3Y-TZP from Tosoh corporation, with 6 mm of diameter
- Sliding distance (total covered distance during the all test) : 50 m
- Load : 20 N
- Amplitude (distance covered on the zirconia tested disc) : 6 mm
- Mode : linear reciprocating
- Speed : RPM = 120 min^{-1} (=0,01 m/s)

Tribological experiments allow obtaining, at the given experimental conditions the wear mode, the wear rate and the coefficient of friction. The linear reciprocating test mode has been chosen because it represents the easiest way to calculate the specific wear rate and the coefficient of friction.

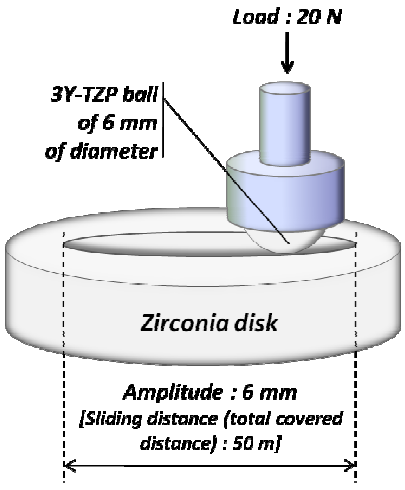

Figure 15: scheme of the ball-on-disk wear test

2.4.1 Specific wear rate

The specific wear rate is expressed in $mm^3.N^{-1}.m^{-1}$ and represents the normalized removed volume for the total covered distance called the sliding distance.

In the present work, this tribological characteristic has been calculated using a confocal microscope, linked to a Lext imaging software.

The removed volume has been calculated twice for each sample. In equation 5, 6000 represents the length of the imprint (µm) and 192 is the height of the picture (µm) taken to perform this calculation.

$$V_{tot} \quad \left(mm^3\right) = \frac{V_{tot1} + V_{tot2}}{2} \times \frac{6000 \times 10^{-9}}{192} \qquad \text{(Eq. 5)}$$

The specific wear rate has been then calculated using the following equation.

$$specific \quad wear \quad rate \quad \left(mm^3 / Nm\right) = \frac{V_{tot}}{F\left(N\right) \times sliding \quad dis\tan ce\left(m\right)} = \frac{V_{tot}}{100} \qquad \text{(Eq. 6)}$$

2.4.2 Coefficient of friction

The coefficient of friction corresponds to the ratio of friction to normal force and it is a dimensionless scalar value. It is an empirical measurement because it has to be experimentally determined to be known. This characteristic is directly given by a computer linked to the tribological test machine.

2.5 Characterization

2.5.1 Microscopy

2.5.1.1 Optical microscopy

Optical microscopy mode has been used on the confocal microscope. The optical microscope is often referred to the "light microscope" and uses visible light and a system of lenses to magnify images of small samples. There are two basic configurations of optical microscope in use, the simple (one lens used for magnification) and compound (many lenses).

Optical microscopy permitted to calculate the Vickers hardness the fracture toughness and to evaluate the microstructural changes after nitridation. Using the DIC (Differential Interference Contrast) filter, the optical microscope permitted to take pictures of the cross sections and the surface of the samples.

2.5.1.2 Confocal microscopy

The principle of confocal microscope [Fig. 16] is as follows. At the focal plane of the objective lens, an objective focuses an expanded light-beam to a small spot on the sample. The objective collected the reflected light from the illuminated volume of the specimen, which is then reflected by a beamsplitter towards a pinhole arranged in front of the detector. Information which does not originate from the focus level of the microscope objective is faded out by this arrangement contrary to the light from the focal plane, which is focused on the detector pinhole and registered by the detector.

The advantage of out-fading information from above or below the focal plane enables the confocal microscope to perform depth-dependent measurements: optical tomography

becomes possible. A genuine 3D-image can be processed by confocal scanning of sequential levels.

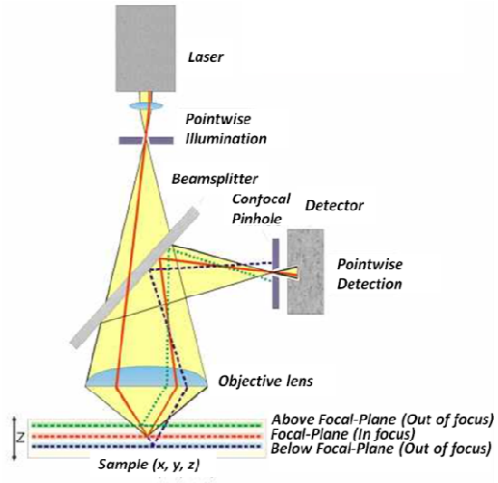

Figure 16: principle of confocal microscopy

In the present study, a confocal Olympus Lext microscope has been used to calculate the removed volume during tribological tests, and then to deduce the specific wear rate.

2.5.1.3 Scanning Electron Microscopy

The scanning electron microscope (SEM) [Fig. 17] is a type of electron microscope that images the sample surface by scanning it with a high-energy beam of electrons in a raster scan pattern. The electrons interact with the atoms that make up the sample producing signals that contain information about the sample's surface topography, composition and other properties such as electrical conductivity.

This type of microscopy has been used to take pictures of the worn surfaces from the tribology tests that permitted to determine the wear mechanisms.

The types of signals produced by an SEM include secondary electrons, back scattered electrons (BSE), characteristic x-rays, light (cathodoluminescence), specimen current and transmitted electrons. In the present work, only secondary electrons and back-scattered electrons are useful for information that are required.

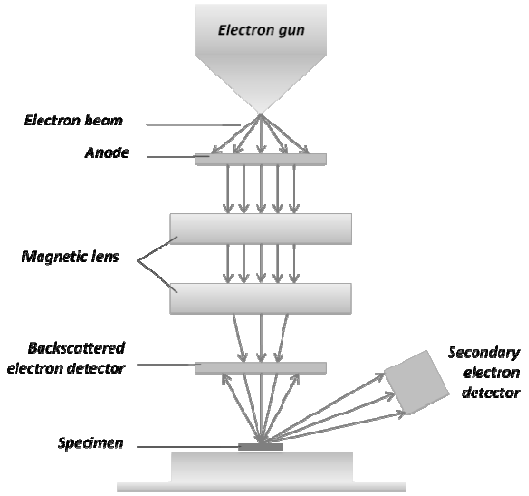

Figure 17: principle of Scanning Electron Microscope

The most common imaging mode collects low-energy (< 50 eV) secondary electrons that are ejected from the k-orbitals of the specimen atoms by inelastic scattering interactions with beam electrons. The amplified electrical signal output by the photomultiplier is displayed as a two-dimensional intensity distribution that can be viewed and photographed on an analogue video display, or subjected to analog-to-digital conversion and displayed and saved as a digital image. This process relies on a raster-scanned primary beam. The brightness of the signal depends on the number of secondary electrons reaching the detector. Thus steep surfaces and edges tend to be brighter than flat surfaces, which results in images with a well-defined, three-dimensional appearance. Using this technique, image resolution less than 1 nm is possible.

Backscattered electrons (BSE) consist of high-energy electrons originating in the electron beam that are reflected or back-scattered out of the specimen interaction volume by elastic scattering interactions with specimen atoms. Since heavy elements (high atomic number) backscatter electrons more strongly than light elements (low atomic number), and thus appear brighter in the image, BSE are used to detect contrast between areas with different chemical compositions. However, strong topographic contrast is produced by collecting back-scattered electrons from one side above the specimen using an asymmetrical, directional BSE detector; the resulting contrast appears as illumination of the topography from that side. Semiconductor detectors can be made in radial segments that can be switched in or out to control the type of contrast produced and its directionality.

Backscattered electrons can also be used to form electron backscatter diffraction (EBSD) image that can be used to determine the crystallographic structure of the specimen.

2.5.2 Vickers (micro-) indentations

2.5.2.1 Vickers hardness

Hardness of a material represents its penetration resistance by another material.

The Vickers hardness test method consists of indenting the tested material with a diamond indenter, in the form of a pyramid with a square base and an angle of 136 degrees between opposite faces subjected to a load of 1 to 100 kgf [Fig. 18]. The full load is normally applied for 10 to 15 seconds. The two diagonals of the indentation left in the surface of the material after removal of the load are measured.

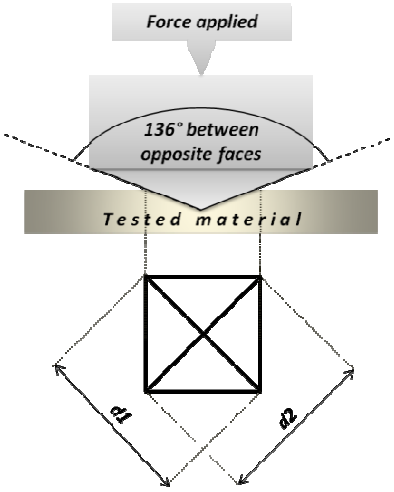

Figure 18: principle of Vickers indentation for hardness determination

Vickers hardness is expressed as shown in the equation 7.

$$H_v(GPa) = \frac{2F.\sin(136/2)}{d^2} = 1{,}854 \times \frac{F}{d^2} \qquad \text{(Eq. 7)}$$

In the equation 7, F is the force applied in kgf and d represents the diagonal average in meters.

In the present work, as the load is given in kpounds, Vickers hardness is calculated using the following expression [Eq. 8].

$$H_v(GPa) = 1{,}854 \times \frac{9{,}81.F}{d^2} \quad \text{(Eq. 8)}$$

The load used to determine surface hardness of 1400°C, 1500°C and 1600°C samples was 1 kpound, and 0,25 kpound (micro-hardness) was the load applied to draw a map of hardness at the cross section (from the surface to the bulk) for the samples sintered at 1400°C and 1600°C, previously incorporated in bakelite and polished as explained in (§ 2.1.4) and as shown on figure 19. For those latter, indentations have been performed from the surface up to a depth of 100 µm, with steps of 20 µm.

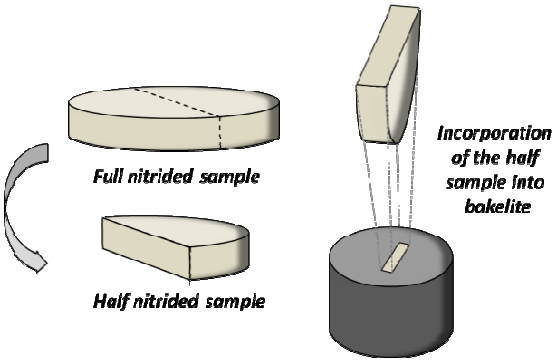

Figure 19: incorporation of half sample into bakelite

2.5.2.2 Fracture toughness

Fracture toughness is the resistance of a material to crack propagation. It is one of the most important properties of any material for virtually all design applications. Fracture exists in 3 different modes [Fig. 20]. For the present study, only the mode I has been taken into account, because it is the most found mode in the material tested. Fracture toughness is a very important material property since the occurrence of flaws in ceramics materials is not completely avoidable in the processing, fabrication, or service of a material.

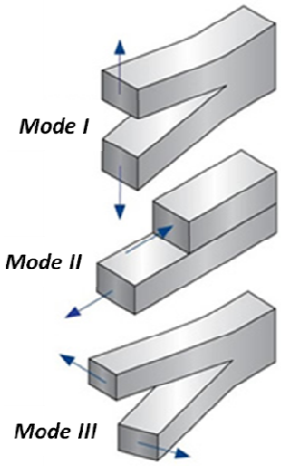

Figure 20: 3 modes of fracture toughness

As for hardness, fracture toughness has been determined by Vickers indentations using the micro-fracture indentation (MI) method[44], but, for the material used in the present work, it requires a higher load (30 kpounds) than for the Vickers hardness, so radial cracks (fissures) can be observed as on the following figure [Fig. 21].

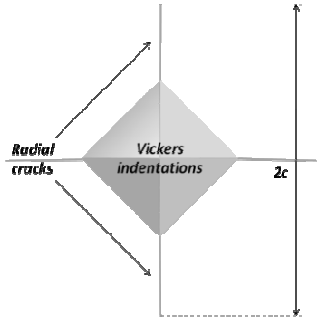

Figure 21: Principle of Vickers indentations for fracture toughness determination

In order to obtain the fracture toughness, hardness was first calculated using the equation 8, and then the following expression was applied.

$$K_{IC}\left(MPa.\sqrt{m}\right)=\beta.\left(\frac{F.H_v}{4c}\right)^{1/2} \qquad \text{(Eq. 9)}$$

$$with \quad \beta=0{,}025\left(\frac{E}{H_v}\right)^{0{,}4} \qquad \text{(Eq. 10)}$$

In the equations 9 and 10, K_{IC} is the fracture toughness, β is a dimensionless parameter, F is the load applied in kpounds, Hv is the Vickers hardness (GPa), E is the Young modulus of the material (GPa), and c is the length of the radial cracks (m).

2.5.3 X-Rays diffraction

2.5.3.1 Principle

Diffraction can occur when electromagnetic radiation interacts with a periodic structure whose repeat distance is about the same as the wavelength of the radiation. Visible light, for example, can be diffracted by a grating that contains scribed lines spaced only a few thousand angstroms apart, about the wavelength of visible light. X-rays have wavelengths on the order of angstroms, in the range of typical inter-atomic distances in crystalline solids. Therefore, x-rays can be diffracted from the repeating patterns of atoms [Fig. 22] that are characteristic of crystalline materials.

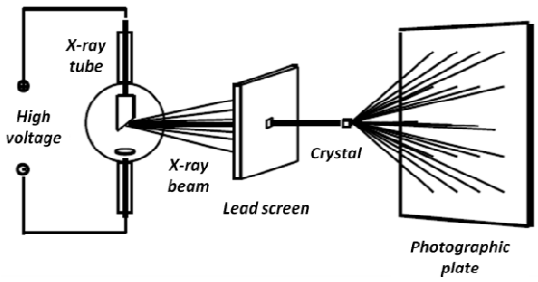

Figure 22: schematic of x-rays diffraction

2.5.3.2 Bragg's law

Bragg's law (Eq. 11) provides the condition for a plane wave to be diffracted by a family of lattice planes.

$$n.\lambda = 2d.\sin\theta \qquad \text{(Eq. 11)}$$

In this equation, λ is the wavelength and is equal to 0,154060 nm (Cu-Kα radiation) and θ is the Bragg's angle (between the wave-vector of the incident plane wave and the lattice planes). d represents the inter-planar distance as shown on the figure 23.

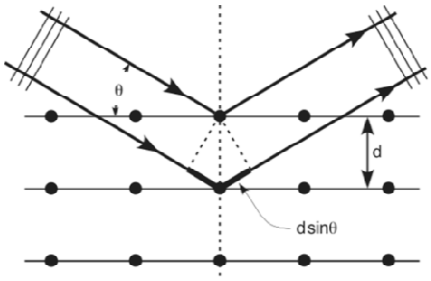

Figure 23: schematic of x-rays diffraction

The incoming beam (coming from upper left on figure 23) causes each scatterer to re-radiate a small portion of its energy as a spherical wave. If scatterers are arranged symmetrically with a separation d (inter-planar distance), these spherical waves will be in synch (add constructively) only in directions where their path-length difference 2d.sinθ equals an integer multiple of the wavelength λ (n). In that case, part of the incoming beam is deflected by an angle 2θ, producing a reflection spot in the diffraction pattern.

2.5.3.3 Uses

X-Rays diffraction results have been analyzed with the software Origin®, to make the following calculations.

2.5.3.3.1 Lattice parameters

X-rays diffraction has been used to calculate the change of lattice parameters a and c produced by nitridation. In order to identify the planes for the lattice parameters calculation, table 8 was used, which corresponds to tetragonal zirconia and shows to plane/angle correspondence for pure zirconium oxide in tetragonal system.

2 theta (°)	Intensity	h k l	2 theta (°)	Intensity	h k l
30.223	*999*	101	68.623	*3*	212
34.570	*81*	002	72.919	*15*	004
35.272	*124*	110	74.592	*37*	220
42.975	*14*	102	78.350	*3*	104
50.219	*320*	112	81.733	*64*	213
50.739	*171*	200	82.544	*31*	301
53.935	*1*	201	83.676	*24*	114
59.274	*106*	103	84.886	*17*	222
60.203	*200*	211	85.289	*15*	310
62.852	*47*	202			

Table 8: X-Rays diffraction, plane/angle correspondance for tetragonal phase in pure zirconium oxide

To obtain *a* and *c* parameters, the equation 12 has been used, which corresponds to tetragonal crystal system.

$$\frac{1}{d^2} = \frac{h^2 + k^2}{a^2} + \frac{l^2}{c^2} \quad \text{(Eq. 12)}$$

In this equation, h,k and l are the Miller indices.

In order to calculate the a parameter, a peak which plane is under the form of hkl = xy0 is required, according to the equation 12. The peak chosen is hkl = 220.

In this case, equation 12 becomes:

$$\frac{1}{d^2} = \frac{h^2 + k^2}{a^2} + \frac{l^2}{c^2} \rightarrow a = \sqrt{8}.d \quad \text{(Eq. 13)}$$

As tetragonal and cubic systems belong to different space groups, to extrapolate the tetragonal a parameter to the pseudo-fluorite structure, this is multiplied by the square root of 2, as shown in equation 14.

$$a = \sqrt{8}.\sqrt{2}.d \quad \text{(Eq. 14)}$$

To determine the c parameter, the reasoning is the same, a peak which plane is under the form of hkl = 00x is required, and the peak chosen is hkl = 004.

The equation 12 becomes:

$$\frac{1}{d^2} = \frac{h^2 + k^2}{a^2} + \frac{l^2}{c^2} \rightarrow c = 4.d \qquad \text{(Eq. 15)}$$

For the *a* parameter as well as for the *c* parameter, the Bragg's law [Eq. 11] is used to determine the inter-planar distance d.

Once the *a* and *c* lattice parameters are known, it is possible to determine the tetragonality of the phase, which is the ratio between *a* and *c* parameters: when the tetragonality decreases and tends to the value 1, it means that *a* and *c* parameters converge toward the same value a_c and the phase tends to be fully cubic. It is calculated with the following expression.

$$tetragonality = \frac{c}{a} \qquad \text{(Eq. 16)}$$

2.5.3.3.2 Monoclinic content

X-Rays diffraction tests have been performed also to determine the monoclinic phase content. This result will inform about the effect of nitridation on retarding aging process. On X-Rays diffraction patterns, peaks correspond to different planes of different phases. Using the software Origin®, it is possible to calculate the area under each peak, and to determine the phases fraction. The range of Bragg's angle used to determine the monoclinic content was from 2θ = 27° to 2θ = 33°. In this range, $(-111)_m$, $(101)_t$ and $(111)_m$ were detected, depending on the samples. Gaussian fit single peak function has been used to calculate the area under the considered peaks. The monoclinic phase content, X_m, was calculated using the Garvie and Nicholson method[45].

$$X_m(\%) = \frac{I_{m(-111)} + I_{m(111)}}{I_{m(-111)} + I_{m(111)} + I_{t(101)}} \qquad \text{(Eq. 17)}$$

In equation 17, I_t and I_m represent the integrated intensity (area under the peaks) of the tetragonal (101) and the monoclinic (-111) and (111) peaks. The monoclinic volume fraction, V_m, was then calculated with the formula of Toraya and co-workers[46]:

$$V_m = \frac{1{,}311.X_m}{1 + 0{,}311.X_m} \qquad \text{(Eq. 18)}$$

3. Results and discussion

3.1 Microstructure

3.1.1 Morphology changes

As it has been explained in the introduction chapter, during nitridation process, a cubic or t' phase layer appears at the surface of the samples, depending on the nitridation temperature.

Figure 24 shows the cross sections of 3Y-TZP nitrided at different temperatures. The main observation that can be made according to the micrographs is that a phase with bigger grains is present at the surface of the samples nitrided at 1600°C. This result has been found by Chung and co-workers[32]. For lower temperatures (1400°C and 1500°C), the surface does not have grains bigger than in the interior of the samples: according to the microstructures, it does not seem that there is a formation of a layer.

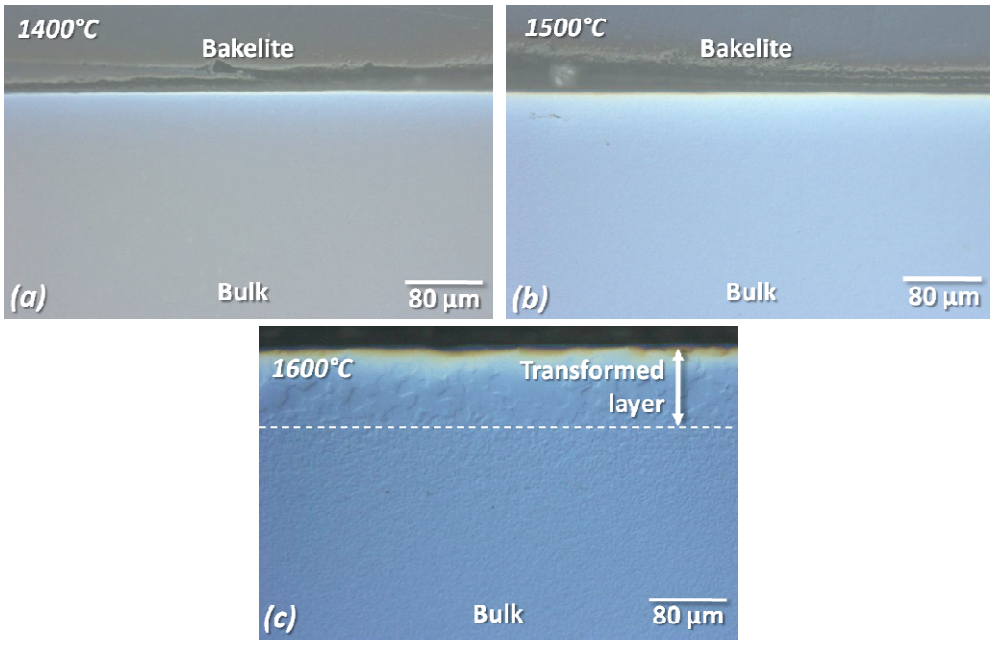

Figure 24: Micrographs showing the cross section of 3Y-TZP specimen after heat treatment with ZrN powder for 1 hour at (a) 1400°C, (b) 1500°C, and (c) 1600°C

3.1.2 Thickness

No layer formation is formed for the samples nitrided at 1400°C and at 1500°C, according to the microstructural observations. The thickness of the surface layer that appears during the doping process has only been detected and calculated for the specimen heat-treated at 1600°C. In this case, the thickness found is 77,0 ± 4,2 µm.

Feder and co-workers[33] have found that for a nitridation process at 1650°C for 1 hour in the same experimental conditions as in the present study, the thickness of the transformed surface layer of 2,5Y-TZP sample was 250 µm, which corresponds to the zone I (at the surface); for the region II, which extends to the interface between the above layer and the bulk, they observed a thickness of 450 µm. The difference of thickness of the outer-most layer with the present study may be explained: (i) by the nitridation temperature, (ii) by the difference of yttria content used in the raw material and/or (iii) by the fact that Feder and co-workers nitrided cylindrical rods, while in this work the samples have disc shape.

Chung and co-workers[32] analyzed the dependence of the surface layer thickness according to the nitridation temperature. They found that for the sample heat-treated at 1600°C for 2 hours, the thickness of the outer-most layer was 100 µm, and for the specimen nitrided at 1700°C for 2 hours, the surface layer had a thickness of 200 µm. In the present study, the difference of thickness with the result of Chung and co-workers concerning the sample heat-treated at 1600°C, is explained by (i) the nitridation time, which is twice the one that was used in this work and (ii) the fact that they obtained fully cubic phase layer.

3.1.3 Grain size

The grain size of the transformed layer was found to be 13,0 ± 1,6 µm; for the samples nitrided at 1400°C and 1500°C, no change was detected, the grain size at the surface remained to 0,3 µm.

In comparison, Feder and co-workers[33] have also determined the grain size, and for the same experimental conditions as explained above, they have found a surface layer (zone I) grain size of 15 µm, which is similar to the result found in this study . For the region II, they observed a gradient in grain size from 4 to 1 µm. As for the difference of thickness of the surface layer, the divergence in the results can be explicated by: (i) the nitridation temperature, (ii) the content of yttria, and (iii) the nitridation procedure. The gradient in grain size is, in the present study, briefly observable on the microstructure (c) of figure 24; the change between the transformed layer and the bulk is steep with almost no gradual change.

Chung and co-workers[32] worked on the microstructure of nitrided yttria-doped zirconia too. For 3Y-TZP samples heat-treated in nitrogen atmosphere for 2 hours at 1600°C without ZrN powder, they obtained a surface layer (zone I) grain size of 10,8 µm. The lower of grain size they have found could be explained by the absence of compacted ZrN powder during the heat-treatment, even if the nitridation time was twice the one used in the present study. This difference of result shows the importance of the ZrN powder contribution.

3.1.4 Crystal structure analysis

Figure 25 presents the x-rays diffraction of studied samples heat-treated at 1400°C, 1500°C and 1600°C for 24° < 2θ < 76°.

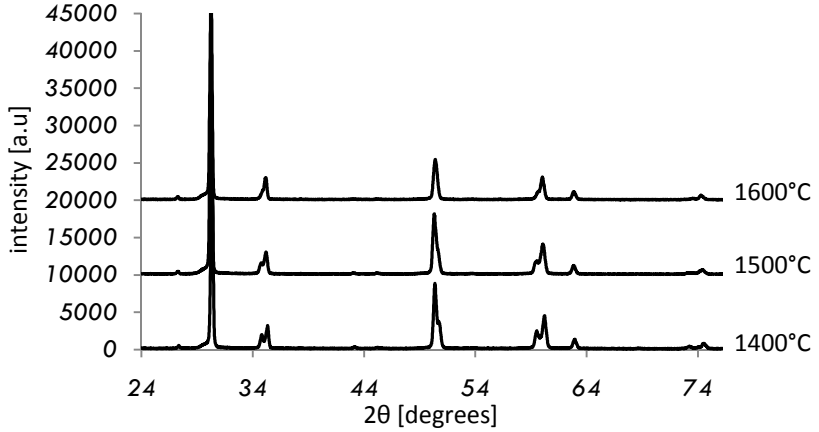

Figure 26: x-rays diffraction (from 24° < 2θ < 76°) for: nitrided at 1400°C, at 1500°C, and at 1600°C

The convergence of the crystallographic planes can be observed on figure 26, which represents the x-rays diffraction for as-sintered sample, nitrided at 1400°C, at 1500°C, and at 1600°C, in detail from 72° < 2θ < 76°. This range has been chosen because it corresponds to a zone where the peaks are not overlaped: the calculations are easier to perform. On figure 26, for each experimental condition, the peak corresponding to 73° < 2θ < 73,5° represents the plane hkl = 004 and the peak defined by 74° < 2θ < 74,5° corresponds to the plane hkl = 400. As those planes tend to converge, the lattice changes of shape to approach a cubic arrangement. It seems that, if others experiments with increased nitridation temperatures are performed, both planes will converge to the plane hkl = 400 that approximately corresponds to 2θ = 73,9° for the cubic zirconia.

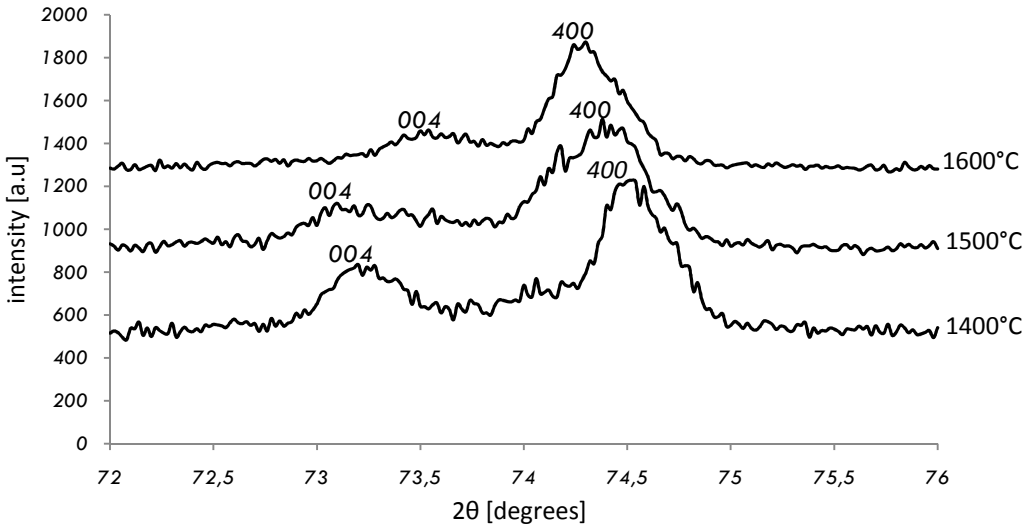

Figure 26: x-rays diffraction (from 72° < 2θ < 76°) for: as-sintered sample, nitrided at 1400°C, at 1500°C, and at 1600°C

The change in lattice parameters resulting from N_2 incorporation and calculated with x-rays diffraction results, is shown in the following table, as well as the tetragonality.

	1400°C	**1500°C**	**1600°C**	**Corresponding planes**
c parameter (Å)	5,1653	5,1612	5,1457	*hkl=004*
a parameter (Å)	5,0882	5,0980	5,1018	*hkl=400*
Tetragonality (c/a)	1,0152	1,012	1,009	

Table 9: a and c parameters and tetragonality results

The comment that can be made regarding those results is that the *c* parameter decreases with the nitridation temperature whereas the *a* parameter increases. This results in the convergence to 1 of the tetragonality, as shown on figure 27.

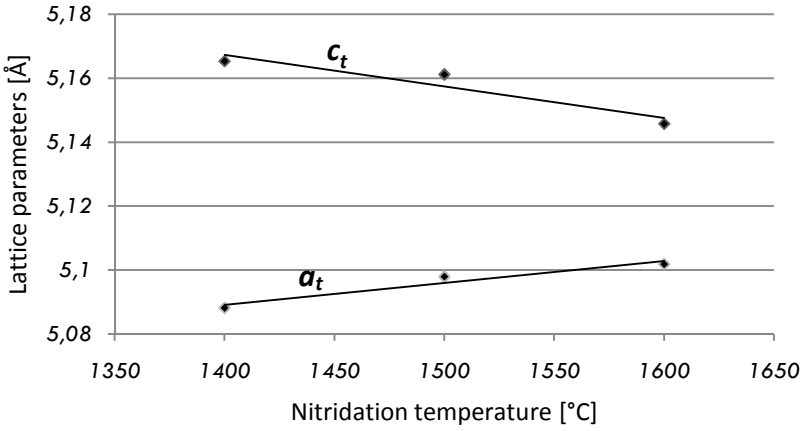

Figure 27: convergence of the lattice parameters, according to the nitridation temperature

3.1.5 Identification of the outer-most layer nature

At this step of the analysis of the surface layer microstructure, it is possible to deduce from the figure 27 and table 3 that the outer-most layer formed during nitridation process is not a cubic phase, because the lattice parameters a and c do not have the same value (no a_c defines this phase) and consequently, the tetragonality is not equal to 1. According to Chung and co-workers[32], when a 3Y-TZP green compact is sintered under a nitrogen atmosphere, a non-transformable tetragonal phase, t', with a low tetragonality (around 1,01[47]) starts to appear at 1400°C and becomes the main phase at 1600°C. In the present work, it is possible to identify the transformed layer as t' phase, given that its tetragonality is lower than 1,01. Samples nitrided at 1400°C and at 1500°C did not form a t' phase, because their c/a ratio is bigger than the referenced value, and much closer to the ratio corresponding to transformable tetragonal phase.

3.1.6 Estimation of the nitrogen content

Using the results of Cheng and co-workers[29] [Tab. 3], it was possible to estimate the nitrogen content for the first 5 µm of depth (what can be detected by x-rays diffraction in θ - 2θ configuration). Knowing the relationship between the tetragonality and the nitrogen content, the values from Cheng and co-workers[29] have been used as shown on figure 28.

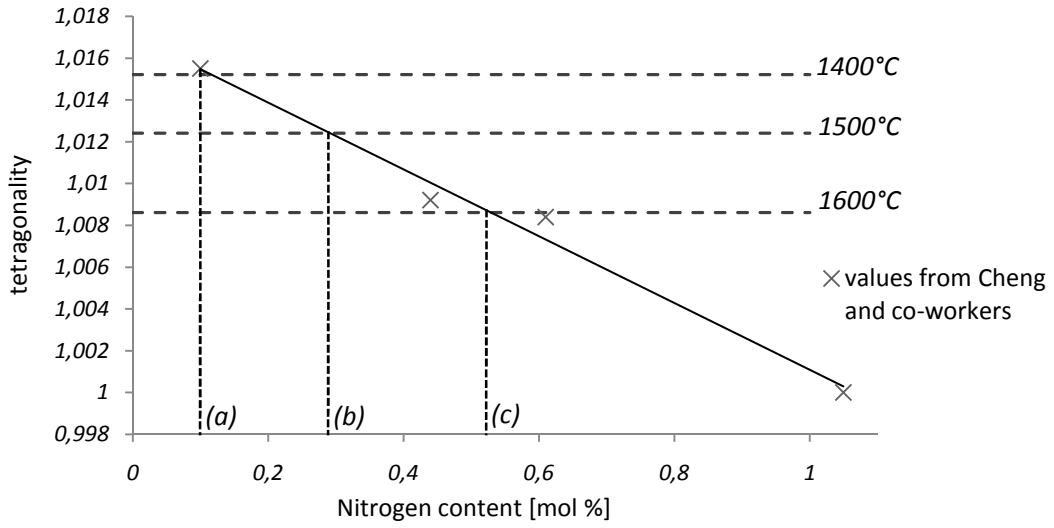

Figure 28: nitrogen content estimation at the first 5 µm of depth for samples nitrided at (a) 1400°C, (b) 1500°C, and (c) 1600°C

It appears, as expected, that the molar percentage of nitrogen at the surface increases with the nitridation temperature: for 1400°C, around 0,1 mol % of nitrogen is present at the surface of the sample, for 1500°C, there is approximately 0,3 mol %, and for a nitridation temperature of 1600°C, there is about 0,55 mol % of nitrogen.

3.2 Mechanical properties

3.2.1 Hardness

3.2.1.1 At the surface

Table 10 shows the hardness values obtained at the surface of the indented samples [Fig. 29], for the three different nitridation temperatures.

	1400°C	**1500°C**	**1600°C**
H_{v1} ***(GPa)***	12,6 ± 0,1	12,9 ± 0,1	15,5 ± 0,5

Table 10: Vickers hardness results at the surface

At the surface of the material, hardness increases with the temperature of doping. More precisely, the increase becomes obvious from a nitridation temperature of 1600°C. This result can be explained by a larger nitrogen content present in such regions and a larger grain size because of the t' phase. As cubic phase has higher hardness than tetragonal, if is considered that t' phase is a gradual structure change from tetragonal to cubic, it is expected to have a hardness value closer to the cubic phase.

Chung and co-workers[32] tested the hardness of the surface layer formed during the nitridation of a 3Y-TZP specimen heat-treated at 1600°C for 2 hours in N_2 atmosphere. They showed the formation of a cubic phase layer at the surface of the sample. As a comparison with the transformed layer in the present work, they obtained a hardness of 13.8 ± 0.2 GPa, which is lower than the hardness of the t' phase.

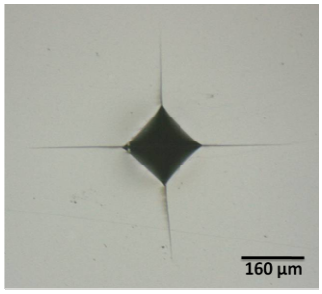

Figure 29: Vickers hardness indentation at the surface of the sample nitrided at 1400°C with a load of 30 kp

3.2.1.2 Along the cross section

Figure 30 shows the results of the micro-hardness tests, in the cross section of the samples nitrided at 1400°C and 1600°C. The first information given by this graph is the difference of micro-hardness depending on the nitridation temperature: the transformed layer of the sample nitrided at 1600°C has a higher micro-hardness (difference of around 2 GPa).

It is important to mention that the Vickers micro-hardness was calculated with 0,25 kpound, it explains why the values obtained in the present case are higher than the ones found using 1 kpound (see § 3.2.1.1). The lower the load, the higher the Vickers hardness, as shown on the following figure. This also explains why the values are different from the ones found in the literature.

The second information, which is the most important, is the decrease of hardness with the depth of the specimen. At 20 µm from the surface, the sample heat-treated at 1600°C has a hardness of 16,2 GPa whereas at 100 µm form the surface, this specimen shows a hardness of 15,2 GPa. Concerning the sample nitrided at 1400°C, $H_{v0,25}$ remains relatively constant.

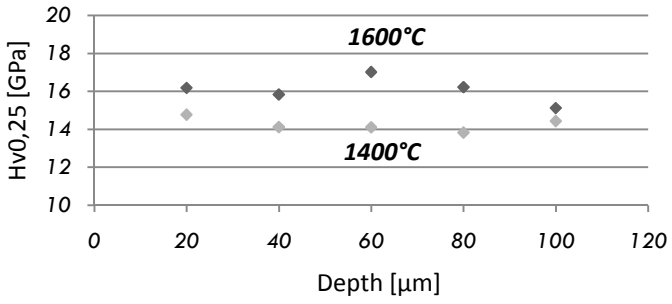

Figure 30: Vickers micro-hardness results in the cross section

Those observations are in accordance with the results of Feder and co-workers[33], who observed a decrease in the Vickers hardness from the surface to the bulk, but their investigation was on a larger depth (from 0 to 1200 µm of depth) than in the present study (from 0 to 100 µm). They found that, at 100 µm of depth, the sample nitrided at 1650°C for

one hour in nitrogen atmosphere and embedded in ZrN powder, the hardness of the material was in a range from 13,5 GPa to 14,5 GPa. This result is in accordance with the value found in the present study for the sample nitrided at 1600°C.

3.2.2 Fracture toughness and chipping

Table 11 presents the indentation fracture toughness values obtained at the surface of the specimens nitrided at 1400°C and 1500°C. These results show similar values of fracture toughness comparing both specimens.

	1400°C	1500°C
K_{IC} (MPa.m$^{-1/2}$)	5,1	5,1

Table 11: Fracture toughness results for sample nitrided at 1400°C

For the sample heat-treated at 1600°C, it appears chipping [Fig. 31] when performing the indentations tests with the loads of 1, 5, 10 and 20 kp. Chipping indicates a very brittle response of the surface, to the indentation test[48]. The difference of behavior during the indentation tests for the sample nitrided at 1600°C is explained by the presence of t' phase, which does not transform to monoclinic under mechanical stress, no transformation toughening occurs.

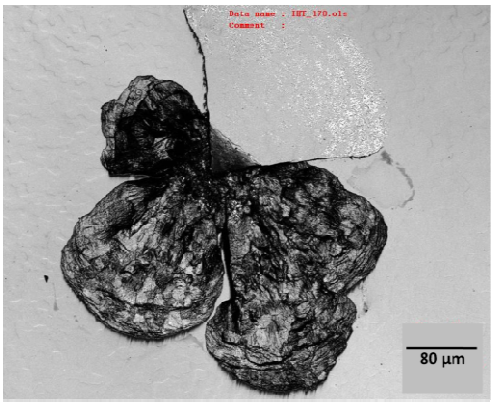

Figure 31: Chipping mechanism for sample nitrided at 1600°C indented with 10 kpounds

3.3 Degradation

X-rays diffractions of degraded specimens are shown on the figure 32 for: as-sintered specimen, heat-treated at 1400°C, at 1500°C, and at 1600°C.

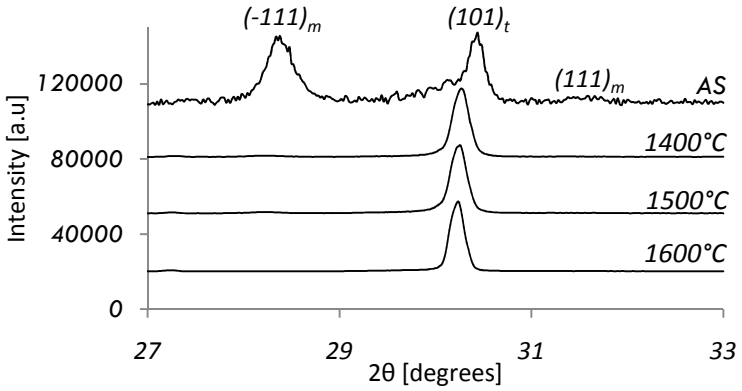

Figure 32: x-rays diffraction of (a) as-sintered sample, (b) heat-treated at 1400°C, (c) at 1500°C and (d) at 1600°C from 27° to 33°

The results given on the figure 32 have been analyzed with the Origin® software in order to determine the monoclinic content. Table 12 shows the percentage of monoclinic phase present at the surface of the samples and the corresponding volume fraction. It can be seen that the as-sintered sample degraded up to 65 % of monoclinic phase, corresponding to a volume fraction of 0,71.

	Monoclinic phase fraction	Monoclinic volume fraction
As-sintered	0,65	0,71
1400°C	0,03	0,03
1500°C	0,03	0,03
1600°C	no monoclinic	no monoclinic

Table 12: monoclinic phase fraction and monoclinic volume fraction in degraded samples

Concerning the samples heat-treated at 1400°C and 1500°C, the presence of monoclinic phase has also been detected, the amount found was 3,0 % (corresponding to a volume fraction of 0,03) for both specimens. The fact that the transformation from tetragonal to monoclinic phase occurred means that the surface was not enough nitrided to produce t' phase at the surface, and that the amount of oxygen vacancies generated at the surface was

lower for those two specimen than for the sample heat-treated at 1600°C. The latter, as shown in the table 12, did not present monoclinic phase at its surface, where the formation of the t' phase had a higher kinetic than for lower nitridation temperature. Guo[15,49] demonstrated that the amount of vacancies is related to the resistance to degradation.

t' is known to be stable against the tetragonal to monoclinic transformation[32] and is the main phase present for a nitridation temperature of 1600°C, which explains that the sample nitrided at 1600°C does not contain any monoclinic phase. As the incorporation of nitrogen in the 1400°C and 1500°C samples is not enough to produce t' phase, their surfaces are still transformable, but in a very less extent.

The results found in the present work show that the nitridation is an efficient way to avoid degradation, depending on the temperature used for the heat-treatment. However, the remaining objective to reach is to find the optimal nitridation temperature in order to obtain a material with good properties and resistant to the hydrothermal degradation. It has been shown that at 1600°C, the hardness had been increased (3 GPa more than for 1400°C and 1500°C), but the fracture toughness couldn't be determined and its decrease is to be expected according to the nature of the surface layer. Concerning hydrothermal degradation, the sample heat-treated at 1600°C has shown a perfect resistance, but the specimens at 1400°C and at 1500°C have only transformed into monoclinic up to 3,0 % of phase fraction. According to the fact that the degradation has been performed to simulate in vivo 90 years of use, it is reasonable to consider that the nitridation at 1500°C represented the optimal temperature condition, for one hour of such treatment.

3.4 Wear behavior

3.4.1 Coefficient of friction

Table 13 shows the coefficient of friction for the different nitridation temperatures. The first observation that can be made from these results is that the values are very similar. However, the highest coefficient of friction is found for the sample nitrided at 1500°C, and the lowest corresponds to the specimen heat-treated at 1600°C.

Nitridation temperatures	**as-sintered**	**1400°C**	**1500°C**	**1600°C**
Coefficient of friction	0,67	0,63	0,69	0,63

Table 13: coefficient of friction for the different nitridation temperatures and for the as-sintered sample

It has been shown by Suh[50] and co-workers that the coefficient of friction depends on the experimental condition and more precisely on the speed. In their investigation, they reported that as-sintered ZrO_2 ball on ZrO_2 disc presents a coefficient of friction in the range of 0,6 to 0,7 for a speed of 0,07 m/s. The results presented in table 13 are in accordance with the ones of Su and co-workers, even if the speed used in the present work was 0,01 m/s. The difference in those results may be explained by the different heat-treatments for three of the tested samples.

3.4.2 Specific wear rate

The specific wear rates found are shown in the table 14. It can be observed that the wear rate for the four specimens is very similar.

As explained in the introduction chapter, it is possible to qualify a wear behavior of mild or severe wear. The latter is observed for a specific wear rate higher than 10^{-4} $mm^3.N^{-1}.m^{-1}$. According to this fact, all the samples studied in this work present a mild wear. The lowest wear rate is observed for the sample nitrided at 1400°C, and the highest concerns the specimen heat-treated at 1600°C.

	As-sintered	1400°C	1500°C	1600°C
Specific wear rate ($mm^3.N^{-1}.m^{-1}$)	$2{,}9.10^{-5}$	$9{,}8.10^{-6}$	$5{,}1.10^{-5}$	$2{,}0.10^{-5}$

Table 14: Specific wear rate values for the different nitridation temperature

However, it is possible to compare the results of the present work with the results of Suh and co-workers[50], who studied the wear behavior of yttria-stabilized ZrO_2 ball on yttria-stabilized ZrO_2 disc using the ball-on-disc type wear test. For a normal load of 20 N, they found a specific wear rate of 10^{-4} mm^3/Nm (for a speed of 0,07 m/s as well as for a speed of 0,14 m/s). Compared with the results in the present study, this value represents a high specific wear rate. According to Rainforth and co-workers[34], the wear rate of zirconia depends sensitively on the sliding speed: it increases by 4 orders of magnitude for an increase in sliding speed from 0,003 to 1 m/s. Consequently, the difference observed between the results obtained in the present work and those found by Suh and co-workers can be explained by the speed: 0,01 m/s for the present study against 0,07-0,14 m/s in their investigation.

It is also possible to compare the results of the present work with the results found by Fischer and co-workers[42], who found that, for fully tetragonal zirconia, mixed tetragonal and cubic zirconia, and fully cubic zirconia sintered at 1500°C, the wear rate were: 7.10^{-7} mm^3/Nm, 3.10^{-6} mm^3/Nm, and 3.10^{-4} mm^3/Nm respectively. Is seems that the cubic phase produced by Fischer is less wear resistant (close to the severe wear) than the t' phase

obtained in the present work. The difference of wear rate may be explained by the grain size parameter: in the present study, the grain size of the 1600°C nitrided sample is around 13 µm whereas the grain size of the cubic phase was found to be in the vicinity of 0,3 µm.

According to the Fischer and co-workers[42], fracture toughness has a strong influence on wear behavior of zirconia ceramics: the wear resistance of zirconia oxide increases with the fourth power of its fracture toughness. In the present work, fracture toughness has only been calculated for the samples nitrided at 1400°C and 1500°C, and 5,1 $MPa.m^{-1/2}$ was found, for both specimens. According to the Fischer's law, values in the range of 10^{-5} mm^3/Nm correspond to 5-6 $MPa.m^{-1/2}$.

3.4.3 Morphology and wear mechanism

Figure 34 shows the SEM images of the worn surfaces for the different nitridation temperatures. The main observation is the difference of surface's aspect between (i) the as-sintered sample, the specimens heat-treated at 1400°C and at 1500°C, and (ii) the sample nitrided at 1600°C.

For the pictures (a), (b) and (c) of figure 34, it can be seen micro-cracking mostly perpendicular to the sliding direction. According to Basu and co-workers[51], those microcracks can be attributed to the stress induced transformation of the tetragonal zirconia phase into monoclinic phase, which causes material removal during the wear tests.

Concerning the sample nitrided at 1600°C (picture (d) of figure 34), large area of around 20 µm of size without micro-cracking can be observed. The presence of fracture can also be detected but with a quite less amount than for the other worn surfaces obtained for lower nitridation temperatures. Those large regions are attributed to the plastic deformation occurring during the tribological test, which is the dominating wear mechanism for the specimen heat-treated at 1600°C.

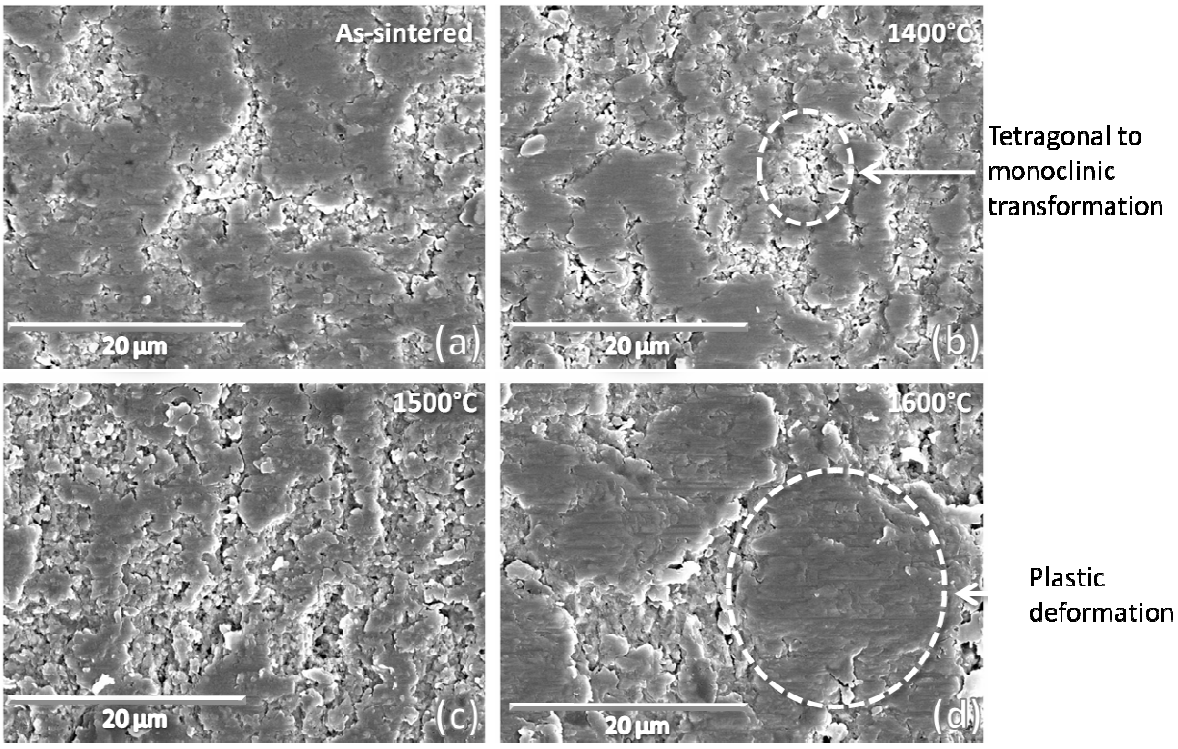

Figure 34: SEM images (x 3000) of worn surface of: (a) as-sintered sample, (b) heat-treated sample at 1400°C, (c) at 1500°C, and (d) at 1600°C

The difference of morphology between both cases described above is related to the composition of the outer-most layer. As it has been explained in the § 3.1.5, the nature of the surface layer is not the same for the different materials tested. During nitridation process, the surface of the specimen nitrided at 1600°C has been transformed into the t' phase, which is not transformable. On the contrary, the other specimens do present tetragonal phase at their surface. Consequently, the stress induced transformation from tetragonal phase to monoclinic phase has occurred during the tribological tests, which represents the main wear mechanism for samples heat-treated at 1400°C and 1500°C.

As mentioned in the § 3.4.2, it is important to remember the influence of the speed used during the wear tests, because it has a sensitive effect on the wear rate, and consequently on the wear mechanism too[34] .

4. Conclusion

In this project, the effect of nitridation on the wear behavior and on the degradation of 3Y-TZP has been investigated.

Nitridation of yttria doped zirconia at 1400°C and 1500°C did not produce transformed layer whereas a t' phase layer of different grain size (13 µm) and different thickness (77 µm) was produced for a nitridation temperature of 1600°C.

Nitridation significantly prevented the hydrothermal degradation, for 30 hours in autoclave, for all conditions tested.

Concerning tribological tests, all samples showed similar coefficient of friction and wear rate, belonging to mild wear regime. Main wear mechanisms for heat-treated specimens at 1400°C and 1500°C were found to be the tetragonal to monoclinic transformation and plastic deformation, and for the sample nitrided at 1600°C, transformation is suppressed and plastic deformation dominates.

5. Environmental impact

The main environmental impact of this project is the use of water during the polishing steps and of electricity during the sintering procedures. The furnace of the brand Hobersal punctually uses current until 10 A in order to increase and maintain the temperature during the sintering process.

6. Cost

The total cost of the project is presented in detail in the following table.

Material used			
Name	**Relative cost**	**Number**	**Cost (€)**
3Y-TZP powder	155,60 € / kg	0,08 kg	12,45
ZrN powder	500 € / kg	0,010 kg	5,00
Diamond paste 30 µm	109,5 € / L	0,20 L	21,84
Diamond paste 6 µm	92,5 € / L	0,1 L	9,25
Diamond paste 3 µm	92,5 € / L	0,1 L	9,25
Colloidal silica	188 € / L	0,20 L	37,60
Bakelite	82 € / kg	0,1 kg	8,20
Lubricant	40 € / L	0,5 L	20,00
		total material cost : *123,59*	
Machines used			
Name	**Relative cost**	**Number**	**Cost (€)**
Furnace	5 € / h	38 h 30 min	192,50
Autoclave	15 € / h	30 h	450,00
Confocal microscope	30 € / h	2 h	60,00
SEM	30 € / h	1 h	30,00
Balance	5 € / h	3 h	15,00
Polishing machines	5 € / h	5 h	25,00
Cutting machine	10 € / h	1 h	10,00
		total machines cost : *782,50*	
Staff required			
Position	**Relative cost**	**Number**	**Cost (€)**
Engineer senior	30 € / h	485 h	14550,00
Project supervisor	60 € / h	2 h	120,00
Laboratory technicians	25 € / h	75 h	1875,00
		total human cost : *16545,00*	
		total cost of the project (€) : 17451,09	

Table 15: total cost of the project

7. Acknowledgment

I first would like to thank Professor Marc Anglada Gomila for having permitted me to study and work in the engineering ceramic field in the “Fracture and fatigue” department at the Technical Superior School of Industrial Engineering of Barcelona (ETSEIB).

I also would like to thank Jorge Antonio Valle for having guided and helped me during the all project execution.

Finally, I would like to thank all the technicians and especially Francesc and Fernando who where there to answer to my questions.

8. References

[1] Piconi, C., Maccauro, G., *Zirconia as a ceramic biomaterial*, Biomaterials 20, 1 – 25, 1999

[2] H. J. Hannink, R., M. Kelly, P., C. Muddle, B., *Transformation toughening in zirconia-containing ceramics*, Journal of American Ceramic Society, 83 [3], 461 – 468, 2000

[3] Bredow, T., *Theoretical investigation of nitrogen substitution in cubic zirconia*, Physical Review B 75, 144102, 2007

[4] Chevalier, J., Gremillard, L., Deville, S., *Low-temperature degradation of zirconia and implications for biomedical implants*, Annual Review of Materials Research, 37, 1 – 32, 2007

[5] Deville, S., Guénin, G., Chevalier, J., *Martensitic transformation in zirconia Part I. Nanometer scale prediction and measurement of transformation induced relief*, Acta Materialia 52, 5697–5707, 2004

[6] M. Kelly, P., L. R. Francis Rose, *The martensitic transformation in ceramics – its role of transformation toughening*, Progress in materials science 47, 463 - 557, 2002

[7] Freed, Y., Banks-Sills, L., Aboudi, J., *On the transformation toughening of a crack along an interface between a shape memory alloy and an isotropic medium*, Journal of the mechanics and physics of solids 56, 3003 - 3020, 2008

[8] Gutzov, S., Lerch, M., *Nitrogen incorporation into pure and doped zirconia*, Ceramics international, 2005

[9] Casellas, D., Feder, A., Llanes, L., Anglada, M., *Fracture toughness and mechanical strength of Y-TZP/PSZ ceramics*, Scripta materialia 45, 213 - 220, 2001

[10] Lu, H.-Y., Chen, S.-Y., *Low-temperature aging of t-ZrO_2 polycrystals with 3 mol% Y_2O_3*, Journal of American Ceramics Society, 70 [8], 537 - 541, 1987

[11] Lange, F. F., Dunlop, G. L., Davis, B. I., *Degradation during aging of transformation-toughened ZrO_2-Y_2O_3 materials at 250°C*, Journal of American Ceramics Society, 69 [3], 237 - 240, 1986

[12] Sato, T., Endo, T., Shimada, M., Mitsudome, T., Otabe, N., *Hydrothermal corrosion of magnesia-partially-stabilized zirconia*, Journal of materials science 26, 1346 - 1350, 1991

[13] Hernandez, M. T., Jurado, J. R., Duran, P., Journal of American Ceramics Society, 74, 1254, 1991

[14] Lawson, S., *Environmental degradation of zirconia ceramics*, Journal of the European Ceramic Society 15, 485 - 502, 1995

[15] Guo, X., Schober, T., *Water incorporation in tetragonal zirconia*, Journal of American Ceramic Society 87 [4], 746 - 748, 2004

[16] Chevalier, J., Cales, B., Drouin, J. M., *Low-temperature aging of Y-TZP ceramics*, Journal of American Ceramic Society 82 [8], 2150 - 2154, 1999

[17] Tsubakino, H., Kuroda, Y., Niibe, M., *Surface relief associated with isothermal martensite in zirconia-3-mol%-yttria ceramics observed by atomic force microscopy*, Journal of American Ceramic Society 82 [10], 2921 - 2923, 1999

[18] Gremillard, L., Chevalier, J., Epicier, T., Deville, S., Fantozzi, G., *Modeling the aging kinetics of zirconia ceramics*, Journal of the European Ceramic Society 24, 3483 - 3489, 2004

[19] Sato, T., Shimada, M., *Transformation of ceria-doped tetragonal zirconia Polycrystals by annealing in water,* American Ceramic Society Bull. 64 [10], 1382 - 1384, 1985

[20] Sato, T., Shimada, M., *Crystalline phase change in yttria-partially-stabilized zirconia by low-temperature annealing,* Journal of American Ceramic Society 67 [10], c-212, 1984

[21] Masaki, T., *Mechanical properties of Y-PSZ after aging at low temperature,* International Journal of High Technology Ceramics 2, 85 - 98, 1986

[22] Kimura, N., Abe, S., Hayashi, Y., Morishita, J., Okamura, H., *Sintering behavior and anti-degradation property of MO_x-doped Y-TZP (M:Cu, Mn, Co, Ni, Zn),* Sprechsaal 122 [4], 341 - 343, 1989

[23] Lawson, S., Gill, C., Smith, J.M., Dransfield, G.P., Egerton, T.A., McColgan, P., *Aging studies of novel Y-TZPs,* Third Euro-Ceramics. Vol. 3: Engineering Ceramics, 507 - 512, 1993

[24] Iio, S., Watanabe, M., Kuroda, K., Saka, H. & Imura, T, *Tetragonal to monoclinic transformation in Y-TZP during low-temperature ageing and its restraint by coating,* Advances in Ceramics. Vol. 24, Science and Technology of Zirconia III, The American Ceramic Society, 49 - 54, 1988

[25] Whalen, P.J., Reidinger, F., Antrim, R.F., *Prevention of low-temperature surface transformation by surface recrystallization in yttria-doped tetragonal zirconia,* Journal of American Ceramic Society 72 [2], 319 – 321, 1989

[26] Cheng , Y.B., Thompson, D.P., *Role of anion vacancies in nitrogen-stabilized zirconia*, Journal of American Ceramic Society 76, 683, 1993

[27] Lerch M., *Nitridation of zirconia*, Journal of American Ceramic Society 79, 2641, 1996

[28] Chung, T.-J., Lee, J.-S., Kim, D.-Y., *Surface nitridation of yttria-doped tetragonal zirconia Polycrystals (Y-TZP): microstructural evolution and kinetics*, Journal of American Ceramic Society 82 [11], 3193 - 3199, 1999

[29] Cheng, Y., Thompson, D. P., *Nitrogen containing tetragonal zirconia*, Journal of American Ceramic Society 74 [5], 1135 - 1138, 1991

[30] Lu, H.-Y., Chen, S.-Y., *Low-temperature aging of t-ZrO2 polycrystals with 3 mol % Y2O3,* Journal of American Ceramic Society 70 [8], 537 – 541, 1987

[31] Lee, I. G., Chen, I. W., *Sintering and grain growth in tetragonal and cubic zirconia,* Sintering '87, 340 – 345, 1988

[32] Chung, T.-J., Song, H., Kim, G.-H., Kim, D.-Y., *Microstructure and phase stability of yttria-doped tetragonal zirconia, Polycrystals heat treated in nitrogen atmosphere,* Journal of American Ceramic Society 80 [10], 2607 - 2612, 1997

[33] Feder, A., Alcalá, J., Llanes, L., Anglada, M., *Microstructure, mechanical properties and stability of nitrided Y-TZP*, Journal of the European Ceramic Society 23 [5], 2955 - 2962, 2003

[34] Rainforth, W. M., *The wear behavior of oxide ceramics-A Review,* Journal of Materials Science 39, 6705 - 6721, 2004

[35] Affatato, S., Spinelli, M., Zavalloni, M., Mazzega-Fabbro, C., Viceconti, M., *Tribology and total hip joint replacement: current concepts in mechanical simulation,* Medical Engineering & Physics 30, 1305 - 1317, 2008

[36] Schmalzried, T., O., Callaghan, J.J., *Current concepts review – wear in total hip and knee replacements,* J Bone Jt Surg [Am], 115 – 136, 1999

[37] Jones, S. M. G., Pinder, I. M., Moran, C. G., Malcolm, A.J., *Polyethylene wear in uncemented knee replacements,* J Bone Jt Surg [Br], 18 – 22, 1992

[38] Pasaribu, H.R., Sloetjes, J.W., Schipper, D.J., *The transition of mild to severe wear of ceramics,* Wear 256, 585 - 591, 2004

[39] Lee, S.W., Hsu, S.M., Shen, M.C., *Ceramic wear maps: zirconia,* Journal of American Ceramic Society 76 [8], 1937 - 1947, 1993

[40] Slonaker, M., Goswami, T., *Review of wear mechanisms in hip implants: Paper II – ceramics IG004712,* Materials and Design 25, 395 - 405, 2004

[41] Willmann, G., Friih, H.J., Pfaff, H.G., *Wear characteristics of sliding pairs of zirconia (Y-TZP) or hip endoprostheses ,* Biomotehk 17, 2157 - 2162, 1996

[42] Fischer, T. E., Anderson, M. P., Jahanmir, S., *Influence of fracture toughness on the wear resistance of yttria-doped zirconium oxide,* Journal of American Ceramic Society 72 [2], 252 - 257, 1989

[43] Deville, S., Chevalier, J., Gremillard, L., *Influence of surface finish and residual stresses on the ageing sensitivity of biomaterial grade zirconia,* Biomaterials 27, 2186 - 2192, 2006

[44] Lawn, B. R., Marshall, D. B., *Hardness, Toughness and Brittleness: an indentation analysis,* Journal of American Ceramic Society 62 [7-8], 347 - 350, 2006

[45] Gravie, R. C., Nicholson, P. S., *Phase analysis in zirconia systems,* Journal of American Ceramic Society 55, 303 - 305, 1972

[46] Toraya, H., Yoshimura, M., Somiya, S., *Calibration curve for quantitative analysis of the monoclinic tetragonal ZrO_2 system by x-rays diffraction,* Journal of American Ceramic Society 67, 119 - 121, 1984

[47] Baither, D., Bartsch, M., Baufeld, B., Tikhonovsky, A., Foitzik, A., Rühle, M., Messerschmidt, U., *Ferroelastic and plastic deformation of t'-zirconia single crystals,* Journal of American Ceramic Society 84, 1755 - 1762, 2001

[48] Lee, S. K., Jensen, R. P., Readey, M. J., *Effect of grain size on scratch damage in Y-TZP ceramics,* Journal of Materials Science Letters 20, 1341 - 1343, 2001

[49] Guo, X., *Hydrothermal degradation mechanism of tetragonal zirconia,* Journal of Materials Science 36, 3737 - 3744, 2001

[50] Suha, M.-S., Chaeb, Y.-H., Kimb, S.-S., *Friction and wear behavior of structural ceramics sliding against zirconia,* Wear 264, 800 - 806, 2008

[51] Basu, B., Vleugels, J., Van Der Biest, O., *Microstructure-toughness-wear relationship of tetragonal zirconia ceramics,* Journal of the European Ceramic Society 24, 2031 - 2040, 2004

9. Appendix

ANNEX A1: Thickness of the surface layer

Thickness measurements (µm)	*Average thickness*
73,0	**77,0 ± 4,2 µm**
80,5	
80,5	
70,5	
73,6	
80,5	
76,1	
81,1	

ANNEX A2: Grain size at the surface

Grain size measurements (µm)	*Average grain size (µm)*
15,1	**13,0 ± 1,6 µm**
11,5	
11,5	
12,7	
14,2	

ANNEX A3: Lattice parameters and tetragonality

	1400°C	*1500°C*	*1600°C*	*planes*
2ϑ (°)	73,241512	73,310096	73,566548	*hkl=004*
intensity	*1988,713136*	*1587,816460*	*1367,000000*	
TETA (radians)	0,639153	0,639751	0,641989	
Sin ϑ	0,596516	0,596996	0,598790	
d (nm)	0,129133	0,129029	0,128643	
c parameter (nm)	**0,516533**	**0,516117**	**0,514571**	
2ϑ (°)	74,538534	74,372035	74,305281	*hkl=400*
intensity	*3222,196976*	*3062,215880*	*3004,000000*	
TETA (radians)	0,650471	0,649018	0,648436	
Sin ϑ	0,605562	0,604405	0,603941	
d (nm)	0,127204	0,127448	0,127546	
a parameter (nm)	**0,508817**	**0,509791**	**0,510183**	
tetragonality	***1,0152***	***1,0124***	***1,0086***	

ANNEX A4: Vickers hardness

	1400°C	*1500°C*	*1600°C*
H_v 1 (GPa)	12,542	12,794	15,005
H_v 2 (GPa)	12,724	12,981	16,087
H_v 3 (GPa)	12,608	12,868	15,619
H_v 4 (GPa)	-	-	15,380
Average (GPa)	**12,625 ± 0,092**	**12,881 ± 0,094**	**15,523 ± 0,453**

ANNEX A5: Fracture toughness

1400°C	**Indentation 1**	**Indentation 2**	**Indentation 3**	
average d (m)	$2{,}051.10^{-4}$	$2{,}036.10^{-4}$	$2{,}034.10^{-4}$	
Hv (GPa)	12,954	13,145	13,179	
average c (µm)	202,439	198,846	203,667	
β	0,075	0,074	0,074	
K_{IC} (MPa.m$^{-1/2}$)	5,124	5,177	5,117	**5,139 ± 0,033**

1500°C	**Indentation 1**	**Indentation 2**	**Indentation 3**	
average d (m)	$2{,}052.10^{-4}$	$2{,}052.\ 10^{-4}$	$2{,}045.\ 10^{-4}$	
Hv (GPa)	12,950	12,950	13,039	
average c (µm)	205,764	204,225	202,723	
β	0,075	0,075	0,075	
K_{IC} (MPa.m$^{-1/2}$)	5,082	5,101	5,124	**5,102 ± 0,021**

ANNEX A6: Monoclinic content

	$I_{m(-111)}$	***$I_{t(101)}$***	***$I_{m(111)}$***	***Monoclinic phase fraction***	***Monoclinic volume fraction***
As-sintered	268,4	157,7	25,1	0,65	0,709
1400°C	182,3	5321,3	-	0,033	0,043
1500°C	150,4	5612,0	-	0,026	0,034
1600°C	-	6830,8	-	0,000	0,000

ANNEX A7: Specific wear rate

	As-sintered	***1400°C***	***1500°C***	***1600°C***
Total volume (mm^3)	0,029	0,0098	0,051	0,020
Specific wear rate (mm^3.N^{-1}.m^{-1})	$2{,}9.10^{-5}$	$9{,}8.10^{-6}$	$5{,}1.10^{-5}$	$2{,}0.10^{-5}$